Title: Spatio-temporal heterogeneity in hippocampal metabolism in control and epilepsy conditions

Authors: BRANCATI[1,2 #] Giulio E., RAWAS[1#] Chahinaz, GHESTEM[1] Antoine, BERNARD[1 ‡] Christophe, IVANOV[1 ‡*] Anton I.

Affiliations :

[1] Aix Marseille Univ, Inserm, INS, Institut de Neurosciences des Systèmes, Marseille, France.

[2] Department of Clinical and Experimental Medicine, University of Pisa, Pisa, Italy.

[#] Contributed equally to this work as first authors

[‡] Contributed equally to this work as senior authors

* Correspondence to anton.ivanov@univ-amu.fr

ABSTRACT

Energy production, mostly via glycolysis and oxidative phosphorylation, which is at the core of cell function, varies in a circadian manner. Whether energy production is tailored to the functional needs of the networks remains poorly understood. The dorsal and ventral part of the hippocampus are involved in different functional circuits. Using metabolic imaging and metabolite sensing, we show that the ventral hippocampus favors aerobic glycolysis over oxidative phosphorylation as compared to the dorsal part in the morning. However, in the afternoon, aerobic glycolysis is decreased and oxidative phosphorylation increased in the ventral hippocampus. In the dorsal hippocampus, the metabolic activity varies less between these two times but is still weaker than in the ventral. Thus, energy metabolism is different in space (along the dorso-ventral axis) and time (in a circadian manner) in the hippocampus. A similar analysis in an experimental model of epilepsy revealed a large alteration of such spatio-temporal organization. In addition to a general hypometabolic state, the spatial difference disappeared in the morning, when seizure probability is low. In the afternoon, when seizure probability is high, the aerobic glycolysis was enhanced in both parts but this increase was stronger in the ventral area. We suggest that energy metabolism is tailored to the functions performed by brain networks, which vary in space and time. In pathological conditions, the alterations of these general rules may contribute to network dysfunctions.

INTRODUCTION.

Energy production in brain cells is assumed to be optimized to the tasks or activities at play in a brain region-specific manner[1, 2]. At the same time the neuronal activity should be adapted to minimize the energy expenditure required for its fueling[3, 4]. Several metabolic pathways are available for energy production, in particular glycolysis and oxidative phosphorylation[5]. Whether specific metabolic pathways are preferably recruited in different brain areas in a task-dependent manner is not known. The hippocampus is an ideal region to test this hypothesis. The dorsal hippocampus (DH) is involved in learning and memory associated with navigation, exploration, and locomotion, whereas the ventral hippocampus (VH) is involved in motivational and emotional behavior[6-8]. These functions are supported by very distinct anatomical[9, 10], morphological[11-13], molecular[14-19] and electrophysiological[12, 13, 20-23] properties of hippocampal cells. The structure of the hippocampus is also highly heterogeneous at the gene level, from its dorsal to its ventral tip[24, 25], which may serve as a substrate for different functional networks related to cognition and emotion to emerge[7, 26, 27] . Given the heterogeneity of the hippocampus, from structure to function, along its dorso-ventral axis, we hypothesized that energy production is different between the VH and the DH.

If energy production is tailored to a given structure-function relationship, we predicted that a change in functional state of the hippocampus should be accompanied by a change in energy production. Epilepsy is a particularly relevant situation to test this hypothesis. The different types of epilepsies are associated with numerous metabolic and bioenergetic alterations[28] . Hypometabolism of epileptic regions is a common signature of mesial temporal lobe epilepsy (TLE) in humans and animal models, such as the pilocarpine model[29, 30]. Importantly, in patients with TLE, only the temporal part (including the hippocampus) is epileptogenic. The temporal part corresponds to the ventral part in rodents, which has been identified as the epileptogenic region in the pilocarpine model[31]. We thus reasoned that there should be a dissociation in the spatial patterns of energy production between the DH and VH in control and epilepsy conditions.

If space (DH vs. VH) is an important variable to consider for hippocampal metabolism, the temporal dimension is another important independent variable. Circadian rhythmicity changes the molecular landscape of cells to anticipate or prepare various life processes such as feeding and sleep[32] . In particular, metabolic genes and metabolites are regulated in a circadian manner, suggesting that energy production is adapted to the cells' needs during the night and day cycle[33]. In fact, circadian clocks and metabolism

are deeply interconnected[34] . In the brain, the best characterized circadian/metabolic system is the Suprachiasmatic Nucleus[35]. Ancillary clocks are also found in other brain regions, including in the hippocampus[35]. Hippocampal functions demonstrate circadian regulation[36], in particular place cell properties[37], long-term synaptic plasticity[38], as well as memory and learning processes[39, 40]. We thus hypothesized that energy production, and more specifically the respective contributions of oxidative phosphorylation and aerobic glycolysis[2], varied as a function of the time of the day. As a first step towards a better understanding of the circadian regulation of metabolism, we considered two time points during the night and day cycle: Zeitgeber 3 (ZT3) and Zeitgeber 8 (ZT8), as they correspond to low and high seizure probability in the pilocarpine model.

In order to test these three hypotheses, we used an *ex vivo* approach to evoke an energy-demanding electrophysiological activity standardized for the three independent variables considered here: time (ZT3/ZT8), space (DH/VH) and perturbation (control/epilepsy). In order to assess the respective contributions of glycolysis and oxidative stress, we used two methods which operate with signals of different nature:

optical, NADH/FAD^+ imaging, and electrochemical, glucose/lactate/oxygen sensing. We found that the DH and VH have distinct time-dependent metabolic signatures (time course of metabolic signals). In experimental epilepsy, there is no more dissociation between DH and VH when seizures have a low probability of occurrence, but the regional difference re-appears when seizure probability is high.

MATERIALS & METHODS

Tissue slice preparation

All animals were kept in colonies, to prevent single housing-induced stress[41]. Adult (2-4 months) FVB male mouse were anesthetized with isoflurane before decapitation at Zeitgeber 3 and 8 (i.e. 10:00 and 15:00, respectively). The brain was rapidly removed (< 30s) and placed in ice-cold artificial cerebrospinal fluid (ACSF). The ACSF solution consisted of (in mmol/L): NaCl 126, KCl 3.5, NaH_2PO_4 1.25, $NaHCO_3$ 25, $CaCl_2$ 2, $MgCl_2$ 1.30, and dextrose 10, pH 7.4. ACSF was saturated in 95% O_2 / 5% CO_2 gas mixture. After cerebellum removal, the two hemispheres were separated. One hemisphere, left or right in alternation, was used to prepare dorsal slices whereas the other hemisphere was used to prepare ventral slices as described in[11]. 350 µm thick slices were obtained with a Leica VT 1200s (Leica Microsystem, Germany). During cutting, slices were submerged in an ice-cold (< 6°C) solution consisting of (in mmol/L): K-gluconate 140, HEPES 10, Na-gluconate 15, EGTA 0.2, NaCl 4, pH adjusted to 7.2 with KOH. Slices were immediately transferred to a dual-side perfusion holding chamber with constantly circulating ACSF and allowed to recover for 2h at room temperature (22°C-24°C).

Synaptic stimulation and field potential recordings.

After recovery, slices were transferred to a dual perfusion recording chamber continuously superfused (6 ml/min) with ACSF contained 5mM of glucose (see explanation below), warmed to 30°C. Schaffer collateral/commissures were stimulated with a bipolar metal electrode connected to a DS2A isolated stimulator (Digitimer Ltd, UK). The electrode tip was placed in *stratum radiatum* between the CA3 and CA2 areas. The extracellular local field potential (LFP) was recorded with a glass micro-electrode filled with ASCF, placed in *stratum pyramidale* of the CA1 area. The signal was amplified 1000 times with an EXT-02F amplifier (NPI Electronic, Germany) operating with a low pass 3kHz filter (DC mode).

We first increased the stimulation intensity (applied at a frequency of 0.15 Hz, using a fixed duration of 200 µs) until reaching the maximum amplitude of the LFP. The current intensity was then adjusted to produce a LFP response at 50-60% of the maximal amplitude. We used this current intensity during trains of stimulation applied at 10 Hz during 10 or 30 s. We tested different train frequencies and found that 10 Hz was optimal because i) it did not damage the slice tissue, even after several (10 trains) stimulation sessions, since it produced identical responses when applied at least 10 times every 5

minutes, ii) it generated LFP responses on each pulse of the train (Fig.1 A), iii) it did not trigger after-discharges, iv) it induced transient change in all metabolic parameters with an amplitude significantly higher (>5 times) than a standard deviation of the baseline (10s before stimulation). In addition, the 10 Hz frequency is within the theta oscillation range and within the seizure discharge range. The 10 s and 30 s durations are also within the range of theta episodes and seizures.

The stimulation intensity necessary to evoke a 50% maximum LFP response was equally variable between 140-300 µA in dorsal and ventral slices (Fig. 1 Ba). In order to assess the response to the stimulation train, we calculated the integral of each LFP response in the train (Fig. 1 Bb) as well as the cumulative integral of all the responses (Fig. 1 Bc), following a previously established procedure[42]. Figs. 1Bb and 1Bc show no difference in evoked electrophysiological responses in ventral and dorsal slices. This allowed to standardize the network response in dorsal and ventral slices, even if their intrinsic excitability may be different (see discussion).

Oxygen, glucose, and lactate measurements.

We used a Clark-style oxygen microelectrode (tip diameter 10 µm; Unisense Ltd, Denmark) to measure slice tissue pO_2. We set the electrode polarization at -0.8 mV and measured the generated current with a PA2000 potentiostat (Unisense Ltd, Denmark). Tissue glucose and lactate concentrations were measured with enzymatic microelectrodes (sensing tip diameter 25 µm, length 0.5 mm; Sarissa Biomedical, Coventry, UK) polarized at 0.5V and driven with the free radical analyzer TBR4100 (WPI, USA). The sensing element of the enzymatic electrode was a platinum/iridium wire coated by a layer of analyte specific enzyme and encapsulated in analyte selective membrane. The enzyme catalyzes oxidation of the substrate producing H_2O_2 which reduction on the surface of platinum/iridium wire provides electrons for the current driven by the polarization potential. Thus, all enzymatic electrodes, independently of their analyte, produced and sensed H_2O_2. Since their selective membrane is permeable to H_2O_2 some of the produced H_2O_2 unavoidably diffuses to the tissue or to another enzymatic electrode located nearby. To minimize possible toxic effects of H_2O_2 when using the glucose sensor, we used ACSF containing glucose at 5 mM instead of 10 mM. With 5mM glucose and a high perfusion rate (6ml/min, and 1 ml chamber volume), the ambient lactate concentration in the slice was 50-250 µM, i.e. nearly two orders of magnitude lower than glucose. At this concentration, the quantity of H_2O_2 produced by the lactate sensor and diffusing in the tissue is very low (i.e. the toxicity is negligible). In each experiment, we

monitored slice viability looking at the stability of LFP responses to single pulse stimulation. Slices were changed if the response amplitude changed by more than 20%.
To avoid an interaction between enzymatic glucose and lactate electrodes, glucose and lactate measurements were done in separate sets of experiments. However, oxygen measurements could be done simultaneously with glucose or lactate ones as the corresponding electrodes have a different design.
Glucose or lactate measurements could not be performed simultaneously with NAD(P)H/FAD^+ because the lactate and glucose oxidase include flavin adenine dinucleotide coenzyme molecules in the active site[43], making the enzymatic sensors sensitive to the excitation light applied for NAD(P)H/FAD^+ imaging.

All electrical signals (LFP, glucose-, lactate-, O_2-generated currents) were digitized using InstruTECH LIH 8+8 acquisition interface (HEKA Electronics, Germany) and stored on the computer hard drive. Stimulation and recording controls were driven with the Patchmaster software (HEKA Electronics, Germany). A second acquisition system, MiniDigi1A interface card and Axoscop software (Molecular Devices, CA), was used to record all signals at a 1 kHz time resolution during the whole duration of the experiment. These recordings were used to estimate the change of sensor sensitivity as a decrease of the base line current generated by the sensors between synaptic stimulations. The oxygen sensor remained stable for several days, whereas enzymatic electrodes lost 20-30% of their sensitivity at the end of each experiment. Continuous recordings were used to estimate with an exponential function the drift in sensitivity to correct lactate and glucose measurements. Between experiments, the enzymatic electrodes were cycled in analyte free ACSF from -500 mV to + 500 mV and back at a rate of 100 mV/s for 3 cycles. They were then polarized to +500 mV during 30 min and calibrated at 5 points in ACSF warmed to 30°C. Glucose and lactate sensors were calibrated before and after each recording session.

NAD(P)H and FAD^+ fluorescence imaging.
NADPH and NADH have similar optical properties, therefore it is expected that NADPH may contribute to the total autofluorescence signal. Because the cellular $NADP^+$/NADPH pool is about one order of magnitude lower than the NAD/NADH pool, in the present study we assume that short-term variations of experimentally detected fluorescent changes responses account for variations in NADH[44]. In the present study, we use the term NAD(P)H for the fluorescent signal.

Slices were epi-illuminated with monochromatic light (pE-2 illuminator, CoolLed, UK) , using 365 nm for NAD(P)H and 440nm for FAD^+. The power of illumination was adjusted to excite the whole thickness of the slice (30-40% for NAD(P)H and 40-50% for FAD^+ of the maximum power of the LED). The emitted light was filtered by 420 nm or 500 nm long pass filter (Omega Optical, Brattleboro, VT) and imaged through a Nikon upright microscope (FN1, Eclipse) with 4x/0.10 Nikon Plan objective using a 16-bit Pixelfly CCD camera (PCO AG, Germany). Because of the low level of fluorescence emission, NAD(P)H/FAD^+ images were acquired every 600-800 ms as 4x4 binned images (effective spatial resolution of 348x260 pixels). The exposure time was adjusted to obtain baseline fluorescence intensity at 50% of the camera dynamic range. Fluorescence intensity changes were measured in *stratum radiatum* near the site of LFP recordings in 3 regions of interest ~1mm distant from the stimulation electrode tip using ImageJ software (NIH, USA). Data were expressed as the percentage changes in fluorescence over a baseline [$(\Delta F(t)/F(t)) \cdot 100\%$] were F(t) is an exponential function of time approximating the base line fluorescence decay estimated using the recording of 1 min base line fluorescence preceding the stimulation (for more details see Ivanov et al., 2014). Signal analysis was performed using IgorPro software (WaveMetrics, Inc, OR, USA).

Experimental model of epilepsy

Adult FVB mice were injected with methylscopolamine (1 mg/kg i.p.) 30 min before the pilocarpine injections. Pilocarpine was repeatedly injected (100 mg/kg i.p.), every twenty minutes, until status epilepticus (SE) was observed. After 90 min of SE, we injected diazepam (10 mg/kg i.p.) to stop SE. All mice then received 0.5 ml NaCl (0.9%) subcutaneously, and again in the evening. During the following days, if required, mice were fed with a syringe.

Statistical analysis and signal processing

To evaluate the difference between metabolic parameters values measured in dorsal and ventral slices we used in parallel two statistical approaches: the non-parametric significance tests and estimation statistic of bootstrap samples. The first approach calculates the probability that the difference would be observed if it does not really exist. Using Shapiro-Francia normality test we verified if the experimental data set could be considered normally distributed. If yes, we applied two tails unpaired or paired t-test. Otherwise, Mann-Whitney or Wilcoxon tests were used to compare unpaired or paired data. This approach although commonly used is dichotomous so it allows only to an-

swer if the difference exists or not without estimating how large the difference is. The second approach, so called bootstrap method[45], consisted to estimate the size of the difference using replication of experimental data set. For this purpose multiple (5000) samples were generated by resampling with replacement of a set of observation obtained for each slice type and their mean values were calculated. Then the distribution of the mean value differences (ventral - dorsal) was constructed. The mean of this distribution and the 95% confidence interval were used as estimator of the difference size. If the confidence interval (CI) included the 0 value the magnitudes of investigated parameter are rather similar in both compared groups. If the CI doesn't include the 0 value, the difference is confirmed and its size is between the bounds of a 95% CI with highest probability to be equal to the mean of the distribution. In the test we reported the difference size as: unpaired or paired *mean difference [lower bound, upper bound of of 95%CI] units*. In some cases when the absolute values were of interest we reported the corresponding mean value and 95% confidence interval obtained using the similar bootstrap procedure.

For unpaired data this type of analysis was performed using estimation statistic web site (*www.estimationstats.com*, see also[46]) while for paired data we used boot package in R language. In both cases the replication number was 5000, and confidence interval was bias corrected. For illustration of data analysis we used estimation plot[46] which shows experimental data set as circles plotted on left hand side Y-axis (black color) and the distribution of estimation parameter (usually ventral -dorsal mean difference) of the bootstrap samples is plotted as gray bell shape area on a floating right hand side (gray color) Y-axis. The mean value of this distribution (black closed circle) as well as its 95% bias corrected confidence interval (black error bar) are also plotted on right hand. The results of significance tests, *p* values, are reported on figures. The asterisk code: *- $0.01<p<0.05$, ** - $0.001<p<0.01$, *** $p<0.001$. We used a two way ANOVA to assess the variability of optical imaging parameters with time.

RESULTS

The ventral hippocampus favors glycolysis over oxidative phosphorylation at ZT3

Metabolic imaging reveals dorso-ventral differences

Nicotinamide adenine dinucleotide (NAD) and flavine adenine dinucleotide (FAD) are essential cofactors in metabolism. They exist in oxidized (NAD^+ and FAD^+) and reduced (NADH and $FADH_2$) forms (please refer to Fig. 10 for summarizing schemes). In the cytosol, NAD^+ is reduced to NADH during the non-oxidative phase of glycolysis and lactate oxidation to pyruvate. In mitochondria, NADH and $FADH_2$ are the main substrates for the respiratory chain; they are essential for ATP production via oxidative phosphorylation. Changes in NAD(P)H fluorescence can reflect both cytosolic and mitochondrial processes, which can be partly disentangled based on their time course[47,48] . Since the trains of stimulation produced a similar electrophysiological response in ventral and dorsal slices (dorsal: 3.8 ± 1.6mV*s; ventral: 4.0 ± 1.6mV*s difference -0.1[-1.3, 1.1] ,mV*s, n=20, see also Fig. 1), we could test possible different metabolic responses between the DH and VH. Stimulations trains (10 s at 10 Hz) induced similar global dynamic changes in NAD(P)H fluorescence in both hippocampal regions (Fig. 2 Aa, left panel): at the onset of the stimulation (gray bar), the fluorescence intensity decreased rapidly (oxidative dip), before rising and overshooting until reaching a peak (reduction peak) after the end of the stimulation, preceding a slow return to baseline (dashed gray line). In our experimental conditions, the initial dip indicates that oxidative phosphorylation is dominating over cytosolic glycolysis, while during the rise to the peak, cytosolic glycolysis is dominating[48](please see also Discussion). The initial dip peaked within ~5-6 s after the train stimulation onset. Its mean amplitude was larger in ventral than dorsal slices (difference 0.7 [-1.1, -0.4]%, n =20, Fig. 2Ab). Although the mean amplitude of the reduction peak was 0.9% larger in ventral than dorsal slices, the 95% confidence interval included the 0 value, [-0.1, 2.1]%, preventing to reach a strong conclusion (Fig. 2Ac, left panel). However in response to a 30 s 10 Hz train, there was a significantly larger reduction peak in ventral slices (mean difference 2.1 [1.2, 3.0]%, n=10, Fig. 2Ac right panel). As expected, the initial dip, which occurs within ~5-6 s was similar for 10 s and 30 s long trains (not shown). We then compared the differences between the two stimulation protocols (Fig. 2B). In the dorsal hippocampus, the 30 s train stimulation lengthened the oxidative dip resulting in a 18 [12, 22]s delay in the onset of the overshoot (Fig. 2Ba, red traces, gray arrow heads and Fig. 2Bc, red circles). However, the overshoot amplitudes remained unchanged (difference -0.1 [-0.4,

0.2]%, n=10, Fig. 2Bb: red circles). In ventral slices, the overshoot onset time was independent of the train duration (difference 1.5[-6.7, 8.8]s, n=10, Fig. 2Ba blue traces, 2Bc blue circles) but the overshoot amplitude was significantly increased in the case of 30 s trains (difference 1.3[0.1, 2.6]% , n=10, Fig.2Bb blue circles).
These results show that ventral CA1 is more active in terms of metabolism. During the first seconds of the stimulation, cells in ventral CA1 mobilize oxidative phosphorylation more than in dorsal CA1 (the initial dip is larger), and then switch to glycolysis (from the overshoot to the peak). When more energy is needed, glycolysis is increased (the peak is enhanced). In contrast, in case of increased activity, the dorsal hippocampus relies longer on oxidative phosphorylation (delayed overshoot) before switching to glycolysis.

Non-fluorescent $FADH_2$ is highly concentrated in mitochondria. It is oxidized to fluorescent FAD^+ in the respiratory chain and can be reduced again in the Kreb's cycle to $FADH_2$. FAD^+ is also reduced at the glycerol-3- phosphate shuttle level as cytosolic NADH gets oxidized (Fig.10). At the onset of the stimulation train, FAD^+ fluorescence increased during 4s (oxidative peak) then declined reaching its minimum (undershoot) after the end of the train (Fig. 2Ca). The FAD^+ oxidative peak was larger in ventral than dorsal slices (difference 0.7 [0.2, 1.1]%, n=10, Fig. 2Cb). The undershoot amplitudes were also larger in ventral than dorsal slices for both 10 s (difference -3.3 [-5.8, -0.6]%, n=10) and 30 s (difference -6.9 [-9.3, -3.7]%, n=10) long stimulation trains (Fig. 2Cc). The paired comparison of FAD^+ transients evoked by 10 s and 30 s long stimulation trains showed that the increased network activation did not affect the amplitude of the undershoot (difference 0.1% [-1.7,1.6], n=10) but delayed the onset time by 6 [3, 10]s in dorsal slices (Fig. 2Da red traces, Db, Dc red circles). In contrast, in ventral slices, (Fig. 2Da blue traces, blue circles on Db and Dc), the undershoot amplitude was increased (difference -3.1 [-0.4, -6.1]% n=10), while the undershoot onset time was not affected (difference 1.2 [-0.5, 4]s, n=10). The FAD^+ results thus support the NAD(P)H ones. Dorsal CA1 appears to rely more on oxidative phosphorylation than ventral CA1, which rapidly switches to glycolysis upon intense network activity. In ventral CA1, the large increase in cytosolic NAD(P)H will produce a large decrease in mitochondrial FAD^+ via the glycerol phosphate shuttle, in addition to the decrease via the Kreb's cycle, both processes regenerating $FADH_2$. In keeping with our hypothesis, the ventral and dorsal CA1 regions behave differently in terms of metabolism: ventral CA1 displays higher metabolic activity than dorsal CA1 and relies on different strategies to produce ATP. In order to assess more directly energy metabolism activity, we measured the extracellular concentrations of lactate, glucose, and oxygen, which are involved in ATP production.

The ventral hippocampus is metabolically more active than the dorsal part in basal conditions at ZT3.

We first assessed whether energy consumption was different under basal conditions between ventral and dorsal slices. In our experimental conditions, O_2 and glucose concentrations are clamped by the ACSF, while lactate is not present in the ACSF. Figure 3A shows the depth profile of pO_2 in slices. The depth with minimal pO_2 value was denoted the 'nadir.' In the perfusion chamber, the ACSF pO_2 was 520-650 Torr. The pO_2 dropped to similar values at the surface of the slice (Fig. 3A): 314±19 Torr in dorsal and to 274±18 Torr in the ventral hippocampi ($p=0.2$, $n=5$). At the nadir (150-180 µm in both slice types), the pO_2 was significantly lower in ventral than in dorsal (159±14 Torr vs 225±17 Torr, $p=0.02$, $n=5$, Mann-Whitney test). Past the nadir, the pO_2 began to increase as the bottom of the slice was also exposed to oxygenated ACSF in the dual perfusion chamber used here. Using two way ANOVA, we found that the type of slice accounts for 34% of the total variance ($F_{(1, 72)}=54.3$, $p<0.0001$). When comparing pO_2 values measured at a depth of 150-200 µm (Fig. 3B, blue circles), we found that the concentration of oxygen was lower in ventral than in dorsal CA1 (difference -80[-140, -30]µM, $n=14$). There is thus a higher level of oxygen consumption in ventral slices in basal conditions.

The design of glucose and lactate sensors only allows measurements from the thickness of the slice. Although glucose is clamped at 5 mM in the ACSF, its concentration was 2.3 mM in dorsal slices and even smaller in ventral slices (difference -0.6 [-0.9, -0.3]mM, $n=14$; Fig. 3B, red circles). This finding is consistent with the difference in tissue pO_2, because oxygen consumption is an indicator of the intensity of oxidative metabolism, which requires glucose. In parallel, we found more lactate (which can only come from cell metabolism in our conditions) in ventral than in dorsal slices (difference 0.08 [0.04, 014]mM, $n=10$; Fig. 3B, green circles), suggesting increased aerobic glycolysis, which end product is lactate, in ventral slices. We conclude that there is a higher metabolic demand in ventral than in dorsal slices in basal conditions. We then assessed the same parameters when the network was stimulated.

Changes in extracellular glucose, lactate, oxygen in response to synaptic stimulation at ZT3.

We used 30 s long stimulation trains as dorso-ventral differences are better revealed in such conditions (Fig. 2), although the results were qualitatively similar with 10 s long

trains (not shown). Figure 3C shows that glucose (red) and oxygen (blue) levels decreased during the stimulation and started to recover after the train stopped. Lactate (green) changed in opposite direction. Since lactate is not present in ACSF, its time course indicates production (via glycolysis), consumption (via oxidative metabolism), and washout by perfusion. Synaptic stimulation led to increased glucose consumption and higher lactate release in ventral as compared to dorsal slices (Fig. 3C-D, difference 0.35 mM [0.1, 0.6] and 0.12 mM [0.07, 0.20], respectively; Mann Whitney test p=0.03 for glucose and lactate, n=6). In contrast, oxygen consumption was identical (difference 0.01 mM [-0.02, 0.05], n=12). These results support the proposal that aerobic glycolysis is increased in ventral as compared to dorsal CA1, while oxidative metabolism is similar when the network is activated.

We then looked at the temporal profile of the responses. To facilitate the comparison, we normalized the traces to the peak amplitude and changed the polarity to make them positive going (Fig. 3E). Oxygen and glucose consumption had very similar time courses in ventral slices, while in dorsal slices the glucose signal was delayed when compared to oxygen (Fig. 3E, bottom panel, dark grays arrows). In ventral slices, oxygen consumption started right after the onset of the synaptic stimulation with a very short time delay (mean 0.6 [0.4, 0.9]s, n=14), which is within the range of the time constant of the oxygen sensor (~1 s). The onset of the glucose response (mean 3[1, 4]s, n=14) did not exceed the sensor latency (3 s). Both signals reached their maximum simultaneously a few seconds after the end of the train (oxygen: mean 4[2, 6]s, n=14; glucose: 6[2, 10]s, n=7). In dorsal slices (Fig. 3E, bottom panel), oxygen consumption started immediately at the train onset (mean delay 0.4[0.1, 0.7]s n=14) and peaked a few seconds after its offset (mean 3.2[2.1, 4.4]s, n=14). Glucose time profile was slower: consumption started 6[3, 12]s later (Mann-Whitney U test: p=0.0003, n=7), and also reached its maximum 23[12, 31]s later (Mann-Whitney U test: p=0.0003, n=7). These results suggest that at the onset of the stimulation, oxidative metabolism (revealed by oxygen consumption) is recruited immediately in both parts of the hippocampus. Whereas, oxygen and glucose consumption are temporally coupled in the ventral part, glucose consumption is delayed in the dorsal part; suggesting the use of other energy sources during this delay. Alternative substrates include lactate, glycogen, amino acids or intermediates of the citric acid cycle. Lactate is unlikely because we did not measure any decrease in lactate concentration at the onset of the stimulation (Fig. 3E, green traces). On the contrary, in both types of slices lactate started to rise 3 s after stimulation onset (difference: 0.2[-1.5, 1.1]s, n=5). Alternate

sources, in particular glycogen, will be addressed in the discussion.
We also compared the changes in metabolite concentration induced by 10s and 30s long trains (Table 1). We found that in both slice types the longer stimulation increased identically the peak amplitude of oxygen transient. In contrast, the increase in glucose consumption was slightly larger in ventral than dorsal slices (87µM vs 56µM, difference: 31[-21, 76]µM), while lactate release was more increased in ventral than dorsal slices (91µM vs 33µM, difference: 49[10, 90]µM).
Together, imaging and molecular sensing experiments reveal major differences between the ventral and dorsal CA1 region of the hippocampus. The intensity of aerobic glycolysis is substantially higher in ventral CA1 in both resting and stimulated states, while dorsal CA1 relies more on oxidative phosphorylation. The coupling between energy metabolism and neuronal network activity thus changes along the dorso-ventral axis (Fig. 10A).

	Dorsal 30s vs 10s Mean diff. [95%CI] *p value* of Wilcoxon paired test	Ventral 30s vs 10s Mean diff. [95%CI] *p* value of Wilcoxon paired test	Ventral vs Dorsal Mean diff of diff. [95%CI]
Oxygen, µM, n=12	47 [36, 58] *p=0.02*	48 [31, 73] *p=0.008*	0 [-20, 28]
Glucose, µM, n=7	56 [33, 104] *p=0.04*	87 [50, 123] *p=0.007*	31 [-21, 76]
Lactate, µM, n=5	33 [17, 54] *p=0.03*	81 [50, 118] *p=0.005*	49 [10, 90] *

Table 1. Mean difference in amplitude of O_2, glucose, and lactate concentration induced by 10 s and 30 s stimulation trains. In both slice types the longer stimulation increased similarly glucose and oxygen consumption (see column Ventral vs Dorsal mean difference of difference), while the gain in lactate release was significantly higher in ventral slices.

Metabolic alterations in experimental epilepsy.

Epilepsy is associated with considerable metabolic modifications in patients and experimental models[29, 30]. Since seizures start from the ventral and not from the dorsal part in the pilocarpine model of epilepsy[31] and since seizures mobilize energy resources, we predicted, a larger dissociation between ventral and dorsal CA1 in the pilocarpine model of epilepsy.

General properties in epileptic mice

Pilo mice weighed less than control or sham (27.1±2.8 g n=26, 33.5±1.8 g n=9, 31.5±1.7 g n=14, respectively $p<0.0001$ ANOVA), but did not present any signs of severe or moderate suffering (the averaged MGS score estimated according to[49] was 0.8 ±0.2 AUs). All mice which experienced status epilepticus (n=21) survived. Pilo mice were not instrumented with EEG telemetry to keep perturbations to a minimum. However, in this model, telemetry measurements performed in another batch of animals show that all pilo mice experiencing status epilepticus develop spontaneous seizures with a low incidence in the morning (2.5-4% between ZT1-3), and a high probability in the afternoon especially at ZT8 (11%) (not shown).

Using a stimulation intensity similar to that used in control slices (260±30µA, n=26) and adjusting it to produce a 70-80% of maximal LFP response, the total integral values of the LFP responses to a 10 Hz 30 s train stimulation were similar in dorsal and ventral slices (mean±sd:1.8±1.0 mV.s and 1.4±0.6 mV.s, respectively, difference 0.5[-0.6, 1.5] mV*s, n=10). These responses were 50% smaller than in control animals (Fig. 2Bc). Since we could normalize the electrophysiological responses in dorsal and ventral slices in pilo animals, we could directly compare metabolic responses. However we could not compare directly metabolic responses between control and pilo mice because the electrophysiological responses could not be normalized between the two conditions.

Loss of regional metabolic NAD(P)H/FAD$^+$ differences in epilepsy at ZT3

Optical NAD(P)H and NAD$^+$ signals had similar general time courses in both ventral and dorsal slices (Fig. 4Aa, Ca). In contrast to control slices, the initial oxidative dip of NAD(P)H (Fig. 4Ab) and oxidative peak of FAD$^+$ (Fig. 4Cb) were identical in ventral and dorsal slices of pilo mice (Table 2). Similarly, the amplitudes of NAD(P)H overshoot and FAD$^+$ undershoot were similar in ventral and dorsal CA1 (Fig.4Ac, Cc, Table2). Other major differences were apparent when comparing 10 s and 30 s long trains. Whereas the onsets of the NAD(P)H overshoot and of the FAD$^+$ undershoot were delayed in dorsal slices only in control animals, the delay was observed in both ventral and dorsal CA1 in pilo mice (Fig.4Bc, Dc, Table 2). In addition, the NAD(P)H overshoot amplitude was not increased anymore in ventral slices for 30 s long trains as compared to 10 s trains (Fig. 4Bb, Table2), while FAD$^+$ undershoot amplitude was significantly increased in both types of slices (Fig. 4Db, Table 2). These results show that, in epileptic conditions, the ventral and dorsal CA1 respond similarly at ZT3. Since

responses show a similar profile in dorsal CA1 in control and epilepsy conditions (e.g. Fig. 2Ba and Fig. 2Da as compared to Fig. 4Ba and Fig. 4Da), we conclude that the ventral hippocampus adopts the metabolic signature of the dorsal part. However, major differences appear as compared to the control condition. In particular, the increase in FAD^+ undershoot whilst the NAD(P)H remains the same suggest an uncoupling between cytosolic and mitochondrial redox states in epilepsy.

NAD(P)H			FAD^+		
	Dorsal vs Ventral			Dorsal vs Ventral	
	Mean dif [95%C.I.]	M-W test, p		Mean dif [95%C.I.]	M-W test, p
Dip amplitude	-0.1[-0.4, 0.2]%	0.38	Peak amplitude	-0.2[-0.6, 0.2]%	0.49
Overshoot amp.			Undershoot amp.		
10s	0.3 [-0.5, 1.4]%	0.65	10s	1.7 [-0.5, 3.7]%	0.13
30s	0.8[-0.1, 1.6]%	0.13	30s	1.4 [-1.9, 4.4]%	0.41
	10s vs 30s			10s vs 30s	
	Mean dif [95%C.I.]	Wilc. paired, p		Mean dif [95%C.I.]	Wilc. paired, p
Overshoot onset			Undershoot onset		
dorsal	12 [8, 16]s	0.02	dorsal	2 [1, 5]s	0.03
ventral	9 [2, 16]s	0.03	ventral	4 [1, 7]s	0.03
Overshoot amp.			Undershoot amp.		
dorsal	-0.1 [-0.6, 0.4]%	0.5	dorsal	-1.9 [-3.1, -1.0]%	0.02
ventral	0.4 [-0.7, 1.5]%	0.4	ventral	-2.2 [-3.5, -1.0]%	0.04

Table 2. Comparison of NAD(P)H and FAD^+ transients recorded in slices of dorsal and ventral hippocampi of pilo mice at ZT3 using estimation statistic and Mann-Whitney U test

Normalization of oxygen, glucose and lactate responses between ventral and dorsal CA1 in epilepsy at ZT3.

We first estimated the basal levels of oxygen, glucose and lactate (Fig. 5A). Although the lactate concentration was significantly lower in ventral than in dorsal slices (difference -43[-60, -23]µM; p= 0.001 Mann-Whitney U test, n=11), the concentrations of glucose and oxygen were similar (glucose: difference -0.12[-0.56, 0.30]mM; p=0.5, n=14; oxygen: difference -0.04[-0.08, 0.01]mM n=18, p=0.2). As for NAD(P)H and

FAD^+, the ventral hippocampus seems to behave like the dorsal part in pilo mice in basal conditions. Although it was not possible to normalize the electrophysiological responses to stimulation trains to compare metabolic responses between control and epileptic animals, we could make the comparison for baseline concentrations (no stimulation condition). Since ventral temporal regions are part of the epileptogenic zone in the pilocarpine model, we hypothesized a large difference between control and epilepsy conditions in the ventral hippocampus. In dorsal slices, the resting state concentrations of glucose and lactate in pilo mice were almost identical to those recorded in control animals (glucose: difference 0.3[-0.2; 0.6]mM, p=0.1; lactate: 14[-20; 40]µM, p=0.2), indicating no or very low effect of the epilepsy condition on the basal level glucose consumption and lactate release. In ventral slices, the difference between control and pilo condition was very large: glucose baseline concentration was 0.7mM higher in pilo group (95%CI [0.4; 1.1]mM, p=0.0008) while lactate concentration was 110µM lower (95%CI [-170; -8]µM, p=0.002). This suggests a large decrease in aerobic glycolysis in the ventral part of the hippocampus in epileptic animals in basal conditions at ZT3. Interestingly, oxidative metabolism was decreased similarly in dorsal and ventral CA1 (pilo vs control difference in basal O_2 concentration in dorsal: 100[40;140] µM, p=0.0007; in ventral: 140[90; 190] µM, p=0.0001). Thus, the altered metabolism in the ventral hippocampus in epilepsy condition erases the regional difference between the dorsal and ventral CA1. This was further confirmed when analyzing the responses to stimulation trains (Fig. 5B).

The mean peak amplitudes of the three metabolites were similar in dorsal and ventral slices (lactate: difference 14[-25, 45]µM; glucose: difference 60[-2, 110]µM; oxygen difference 5[-28, 37]µM). In both types of slices, glucose consumption started more than 10 s after stimulation onset (mean 12[10, 14] s in dorsal, 10[6, 14] s in ventral slices, n=9, no difference between ventral and dorsal, see also Fig. 5C, dark gray arrows). Interestingly, in 7 out of 9 dorsal and 3 out of 9 ventral slices, we observed a positive deflection of glucose at the beginning of the synaptic stimulation (Fig. 5B red traces, arrow head), which interpretation will be addressed in the discussion. The delay in glucose consumption does not mean an increased latency of energy metabolism because the oxygen concentration (Fig. 5C, blue trace) started to decrease immediately at the onset of electrical stimulation independently of the type of slice (mean 0.3[0.1, 0.8]s in dorsal and 1.0[0.7,1.5]s, n=9, no difference between dorsal and ventral) showing a good temporal coupling between electrical activity and oxygen consumption. In both slice types lactate production started to rise a few seconds (mean 6[5, 7]s in

dorsal, 7[6, 8]s in ventral, n=6) after the stimulation onset (Fig. 5, C green trace) but before glucose consumption, suggesting that lactate production uses a substrate different from glucose (as it decreases later), such as glycogen (see Discussion section). Together these results confirm the disappearance of the regional difference between the dorsal and ventral hippocampus in epileptic mice (Fig. 10C). In addition, metabolic responses measured at ZT3 are qualitatively very different between control and epileptic animals (compare Figs. 2-3 with Figs 4-5). Thus, at ZT3, there are important alterations of the metabolic rules in experimental epilepsy as compared to control.

NAD(P)H and FAD^+ fluorescence transients evoked by synaptic stimulation in hippocampal slices of pilo mice prepared at ZT8.

Since pilo mice have a higher probability to have a seizure at ZT8 that at ZT3, we assessed metabolic responses at ZT8 and found that dorso-ventral differences appeared at ZT8. Neuronal network responses to the stimulation were similar in slices of both types (mean ± SD total integral in dorsal: 1.4 ± 0.9 mV*s, in ventral 1.5 ± 0.8mV*s, difference -0.1[-1.0, 0.8]mV*s) allowing direct comparison. The mean NAD(P)H overshoot amplitude was significantly larger (10 s train: difference 1.5[0.5, 2.4]%; 30 s train: difference 2.1[0.5, 3.2]%) while the oxidative dip was smaller (difference 0.33[0.11, 0.51]%) in ventral than in dorsal slices (Fig. 6A). FAD^+ transients (Fig. 6C) were different only in their oxidative peak, which was smaller in ventral slices (mean difference -1.4[-1.9, -0.8]%). The mean undershoot amplitudes were similar for both 10 s (difference -0.7[-4.7, 2.9]%) and 30 s (difference -1.0[-5.1, 2.8]%) long trains. Both NAD(P)H and FAD^+ signals recorded in dorsal and ventral slices responded to the longer train with an increase of the overshoot/undershoot amplitude (Fig.6B and D, double head dashed arrow). The onset time of FAD^+ undershoot was delayed in dorsal slices only by 2 s (Fig.6, Dc), while the onset of NAD(P)H overshoot was not affected by the longer stimulation (Fig. 6, Bc). These results suggest that at 10s train stimulation the dorsal CA1 relies more on oxidative phosphorylation (larger amplitude of oxidative dip/peak of NAD(P)H/FAD^+), while ventral CA1 preferentially uses aerobic glycolysis (larger NAD(P)H overshoot amplitude). However to respond to energy demand induced by longer stimulation the slices of both types recruit aerobic glycolysis (increases in overshoot/undershoot amplitudes). We conclude that dorso-ventral dissociation re-appear at ZT8 in pilo mice (Fig. 10D).

Increased aerobic glycolysis in ventral CA1 in epileptic mice at ZT8.
In non-stimulated conditions, the extracellular concentration of lactate was similar (Fig. 7A, difference 10[-20, 30]µM, n=12), in contrast to ZT3 (Fig. 5A). However, the concentration of oxygen and glucose (Fig. 7A) were significantly lower in ventral slices (glucose: difference -0.4[-0.70, -0.05] mM, n=15; oxygen: difference -0.15[-0.20, -0.09] mM, n=18). Thus, in basal conditions, the ventral hippocampus is more active with enhanced oxidative metabolism at ZT8, in contrast to the lack of differences at ZT3 (Fig. 5). In response to electrical stimulation, we found an increased production of lactate (Fig. 7B, difference 50[10, 80] µM) and increased consumption of glucose (difference 0.23[0.05, 0.40] mM, n=7) in ventral CA1, while oxygen consumption was similar (difference -10[-30, 15] µM, n=13). These results are consistent with the NAD(P)H ones, revealing enhanced aerobic glycolysis in ventral slices (larger overshoot and larger changes in lactate and glucose).
As observed at ZT3, glucose consumption started with a delay (Fig. 7C dark gray arrows). This delay was shorter in ventral than dorsal slices (difference -3.0[-5.0, 0.5] s, p=0.04, n=7, Mann-Whitney test) that suggested a preferential utilization of the extracellular glucose rather than alternative energy substrate (see Discussion). In slices of both types there was no initial rise in glucose concentration as observed at ZT3 (Fig. 5B red trace, arrow head) indicating an improved energetic state (see Discussion). Together, these results suggest a strong circadian alteration in the rules governing energy metabolism along the dorso-ventral axis in epileptic mice. We thus directly compared, the results obtained at ZT3 and ZT8 (Fig. 8).

Circadian alterations in energy metabolism in epilepsy condition.
The NAD(P)H responses were substantially different between ZT3 and ZT8 in ventral and dorsal CA1 in pilo mice (Fig. 8Aa dorsal -warm colors, ventral-cold colors): the initial dip was smaller, the overshoot larger and started earlier at ZT8. Since the data followed a normal distribution (Shapiro-Francia normality test), we performed a variability analysis using a two-way ANOVA (Fig. 8Ab, Ac, Ad). The analysis confirmed that time of the day (ZT3 vs ZT8) was extremely significant for all parameters describing NAD(P)H transients ($p<0.001$ for each parameter), and that there was no interaction between the time of the day and the type of slice (dorsal/ventral). The Bonferroni corrected post-hoc test did not confirm the time dependence of overshoot amplitude in dorsal slice (Fig. 8Ac). The time-dependence of FAD^+ signals was less apparent (Fig. 8Ba) but still significant. Variability analysis showed that both undershoot

parameters, amplitude and onset time, were influenced by the time of the day (two- way ANOVA, p=0.0014 for the amplitude, p=0.0002 for the onset time), while the oxidative peak was not influenced (p=0.06). The Bonferroni corrected post-hoc tests revealed that only the undershoot was larger (p<0.01) and started earlier (p<0.001) at ZT8 in ventral slices (Fig. 8Bc, Bd). These results suggest that aerobic glycolysis is enhanced (larger overshoot/undershoot amplitudes) and starts earlier at ZT8 than at ZT3 especially in ventral slices. However, NAD(P)H and FAD^+ results do not provide enough information regarding a possible circadian regulation of oxidative metabolism, since NAD(P)H oxidative dips were smaller at ZT8 (Fig. 8Ab) while FAD^+ peaks were either larger in dorsal slices or unchanged in ventral slices (Fig. 8Bb). The comparison of the oxygen, glucose, and lactate levels provided the necessary information to interpret the result. Oxygen consumption in stimulation conditions was similar at ZT3 and ZT8 (Table 3 and Fig. 8Ca), while the decreases in glucose concentration were substantially larger at ZT8 than at ZT3 (Table 3 and Fig. 8Cb top). Ventral slices also released more lactate at ZT8, whereas in dorsal slices this parameter was not affected (Table 4 and Fig. 8Cc). Importantly, glucose consumption started early at ZT8 (Table 4 and Fig. 8Cb bottom) in keeping with the facts that the time onset of NAD(P)H overshoots and FAD^+ undershoots occurred earlier. An early glycolysis onset would advance NAD^+ reduction thus masking the oxidative dip, making its amplitude apparently smaller.

	ZT8 vs ZT3 Mean diff. [95%C.I] Mann-Whitney test *p value*	
	Dorsal	Ventral
Oxygen concentration change of amplitude	-5[-25, 17] µM *p=0.8*	-27[-52, 1] µM *p=0.2*
Glucose concentration change of amplitude	0.1 [0.03, 0.28] mM * *p=0.011*	0.28 [0.14, 0.45] mM * *p=0.006*
Glucose consumption onset	-5 [-7, -2] s * *p=0.02*	-6 [-10, -3] s * *p=0.06*
Lactate concentration change of amplitude (release)	24 [-16, 58] µM *p=0.3*	58 [23, 89] µM * *p=0.02*

Table 3. Difference between metabolic parameters of slices prepared at ZT3 and ZT8 from pilo animals.

We conclude that aerobic glycolysis is accelerated and enhanced at ZT8 as compared to ZT3, in both ventral and dorsal CA1, while the intensity of oxidative metabolism is similar at both time points (Figs. 10C & D). Since metabolic properties are different between ZT8 and ZT3 in epilepsy conditions, we assessed whether metabolic properties are time-dependent in control animals.

Circadian regulation of metabolism in CA1 in control animals

The comparison of dorsal and ventral slices obtained at ZT8 led to the same conclusion as those prepared at ZT3 in control animals. The intensity of aerobic glycolysis was substantially higher in ventral CA1 in both resting and stimulated states (stimulation intensity 210-280µV, LFP integrals 4.3 ± 1.8 mV*s in dorsal, 4.0 ± 1.5 in ventral, difference -0.4[-0.8, 1.1] mV*s n=12), while dorsal CA1 relies more on oxidative phosphorylation (Fig. 9 and Table 4 for statistical analysis). The dorso-ventral dissociation is thus maintained at ZT8 in controls.

Clear differences appeared between dorsal and ventral CA1, when we compared the metabolic responses obtained at ZT3 and ZT8. In dorsal slices, the parameters characterizing NAD(P)H and FAD^+ responses (Fig. 9A and B) were similar at ZT3 and ZT8 in dorsal slices, except for a shorter overshoot onset time (Fig. 9Ac). The steady state concentration of metabolites showed a decreased metabolism at ZT8: the levels of glucose (Fig. 9Ca) and oxygen (Fig. 9Cc) were higher (lower consumption), while lactate (Fig. 9Cf) was lower. In stimulation condition, although glucose uptake was independent of time (Fig. 9Cb), oxygen consumption (Fig. 9Cd) and lactate release (Fig. 9Cf, Cg) were smaller at ZT8. There is thus a weaker metabolic activity in dorsal slices at ZT8 than at ZT3.

The situation was very different in ventral slices, in which both oxidative phosphorylation (FAD^+ peak) and aerobic glycolysis (NAD(P)H overshoot amplitude and onset, FAD^+ undershoot amplitude and onset) were enhanced at ZT8 as compared to ZT3 (Fig. 9A and B dark color traces vs light colors). Interestingly, the steady state concentration of metabolites showed a decreased metabolism at ZT8 as for dorsal slices: the levels of glucose (Fig.9 Ca) and oxygen (Fig.9 Cc) were higher (lower consumption) while lactate (Fig.9 Ce) was lower.

In response to synaptic stimulation, ventral slices consumed oxygen similarly at both time points (Fig. 9Cd) but absorbed more glucose (Fig. 9Cb) and released substantially less of lactate (Fig. 9Cg) at ZT8 than at ZT3. Moreover in 4 from 5 experiments, lactate

concentration decreased at the onset of synaptic stimulation (Fig. 9Cf, gray arrowhead). Since glucose uptake was not delayed as compared to ZT3 (Table 4,"Glucose consumption onset"), the observed lactate dip may indicate that lactate consumption dominated over its production. We can rule out a downregulation of lactate production, because it would led to a decrease in the amplitude of NAD(P)H overshoot; whilst we observed the reverse (Fig. 9Aa, c). When consumed, lactate is transformed to pyruvate that requires NAD^+ reduction. The resulting NADH production, occurring at the very start of the stimulation, could mask the increase of the initial NAD(P)H dip (Fig. 9 Aa, Ab). Therefore, since the FAD^+ response clearly showed increased oxidative phosphorylation at the beginning of the response (Fig. 9Ba, Bb), we conclude that this metabolic pathway was increased while aerobic glycolysis is down-regulated at ZT8 as compared to ZT3 in ventral slices (Figs. 10A & B). In contrast, aerobic glycolysis was enhanced in ventral slices at ZT8 in pilo mice.

	ZT8 vs ZT3 Mean diff. [95%C.I] Mann-Whitney test *p value*	
	Dorsal	Ventral
Glucose concentration change of amplitude	0.11 [-0.12, 0.49]mM p=0.08	0.5 [0.15, 0.86]mM* p=0.17
Glucose base line concentration	1.4[1.0, 1.9]mM* p=0.0002	1.32[0.6, 2.2]mM* p=0.04
Glucose consumption onset	2[-3, 8]s p=0.71	1[-1, 2]s p=0.28
Oxygen concentration change of amplitude	-44[-70, -20]µM* p=0.007**	-18[-50, 25]µM p=0.5
Oxygen base line concentration	72[11, 110]µM* p=0.0006***	50 [-1, 84] p= 0.036*
Lactate concentration change	-43 [-68, -23]µM* p=0.01*	-90[-200, -27]µM* p=0.06
Lactate base line concentration	-35 [-70, -6]µM* p=0.4	-80[-140, -42]µM* p=0.03*

Table 4. Difference between metabolic parameters illustrated on Figure 9C.

DISCUSSION

The main findings of the present work are that oxidative metabolism and aerobic glycolysis are differently recruited in space (dorsal versus ventral CA1) and time (ZT3 versus ZT8) in control mice, and that such spatio-temporal organization is modified in experimental epilepsy (Fig. 10). The ventral hippocampus displays a larger dynamic range for energy production than the dorsal hippocampus in both control and epilepsy conditions.

Limitations of the study

We used stimulation trains to assess energy metabolism. In order to remain close to physiologically relevant conditions, we used a 10 Hz frequency, which is within the range of theta oscillations (4-12 Hz), a brain rhythm associated to numerous cognitive and behavioral functions[50] and lengths (10 s and 30 s) that are compatible with the duration of locomotion and REM sleep episodes, for example. The 10 Hz frequency is also within the 0.5-40 Hz band of oscillations found during seizures, which can last between 10 and 30 s. Although artificial, the trains used in the present study are consistent with the synaptic activity CA1 pyramidal cells would experience in physiological and pathological conditions. Electrical stimulation allowed us to normalize the electrophysiological responses, enabling a direct comparison between the dorsal/ventral and ZT3/ZT8 conditions in control animals. However, we could not directly compare the evoked responses between control and epilepsy conditions since the electrophysiological responses were systematically smaller in pilo than in control animals, probably due to the cell loss that characterizes this model[51] . Pharmacological approaches can be used to evoke activity in slices, including the perfusion of carbachol or kainic acid to trigger theta and gamma oscillations[52, 53], respectively , but oscillations are very variable from one slice to another, preventing normalization across conditions. Brain cells must have access to nutrients (glucose, oxygen) and the possibility to eliminate waste products to maintain a healthy state. In the *ex vivo* brain preparation, this goal is achieved thanks to the high rate perfusion of the slice with ACSF on both sides of the slice, which prevents the creation of the zone of hypoxia and hypoglycemia in the middle of the slice, especially during the strong metabolic activity associated with the neuronal network stimulation[42]. We showed previously that in these experimental conditions, the amplitudes of the NAD(P)H dip and of the FAD^+ peak are associated with the activity of oxidative metabolism, because they are directly related to the oxygen

consumption, whilst the overshoot and undershoot components are associated with the activity of cytosolic glycolysis because they are abolished if cytosolic glycolysis is blocked when substituting glucose for pyruvate[42, 48, 54] (see also the pionniering Peter Lipton work[47]). When a lower perfusion rate on one side only is used, the center and bottom slice are in hypoxic and hypoglycemic conditions, reducing oxidative phosphorylation leading to an increase in mitochondrial NADH and $FADH_2$. Consequently, the FAD^+ and NAD(P)H signals are mainly of mitochondrial origin[55], so they are not comparable with those presented in this work.

We chose an *ex vivo* approach because it is not possible in practice to standardize the stimulation in freely moving animals and because oxygen and glucose supply cannot be clamped *in vivo*, due to the variable hemodynamic. In addition, the absorption spectra of oxygenated and deoxygenated blood are different, so the transition from one to the other can affect the NAD(P)H and FAD^+ signals[56] . Finally, invasive equipment would induce astrogliosis and neuroinflammation, which would alter the metabolic state of the brain tissue.

Finally, the methods do not offer enough resolution to distinguish between neuronal and glial cell effects. The oxygen electrode can measure metabolic changes in a small volume of tissue comprising a few cells (sphere of 30 µm in diameter). All the techniques used here integrated metabolic signals over a much larger volume which depth was equal to the thickness of the slice. This difference in spatial scale is probably responsible for some discrepancies observed between the results of the oxygen detection and all the other methods. However the techniques used here allowed us to explore the same metabolic events from intracellular (NAD(P)H/FAD^+ imaging) and extracellular sides. By matching the intra- and extra-cellular signals we obtained important conclusions about the metabolic specificity associated with difference in space (dorsal vs ventral), time (ZT3 vs ZT8) and functional state (healthy vs epileptic brain). The scheme that we propose does not make a distinction between neurons and glial cells thus we summarize our results on a “neuro-glial” cells.(Fig. 10).

We used dorsal and ventral slices, i.e. two gross spatial locations along the septo-temporal axis of the hippocampus. Whilst some coronal slices can give access to both septal and temporal regions simultaneously, the wrong orientation of the Schaffer collaterals prevents using the same protocol. Future studies are needed to determine whether there is a smooth gradient of metabolic properties along the longitudinal axis, as demonstrated for membrane oscillations in entorhinal stellate cells[57], or whether specific domains exist as demonstrated for gene expression along the longitudinal axis

of the hippocampus[24]. In addition, we performed our measurements in distal CA1, far from the stimulating electrodes. Since there is morpho-functional gradient along the transverse axis[58] (from proximal CA1 close to the CA2 to distal CA1 close to the Subiculum), we cannot rule out that the properties of metabolism also vary along this axis. Likewise, these properties may be different in the other subfields (CA2, CA3, dentate gyrus) of the hippocampus.

We used only two time points – ZT3 and ZT8 – because they correspond to a low and high seizure probability in pilo mice, respectively. Yet, even with two time points, we could already evidence differences in control animals, thus providing the proof-of-concept of a circadian regulation of metabolism in the CA1 region of the hippocampus. Further studies are needed to assess metabolic function hour per hour, in particular during the night (active) phase.

We did not instrument pilo animals to monitor seizures. Hence it is possible that spontaneous seizures occurring prior measurement may have altered energy metabolism. We decided not to instrument mice in order to remove two confounding factors: the unknown effects of invasive surgery and anesthesia and the stress induced by single cage housing, which is required for instrumented animals. Single cage housing produces a very severe epilepsy phenotype, while group housing decreases seizure frequency by at least one order of magnitude[41]. Although we cannot rule seizure-induced metabolic alterations, we could still evidence spatio-temporal differences in pilo mice. Obviously, we cannot claim a homology between an animal model and human epilepsy. We were only interested in the broad context of a neuronal network generating spontaneous seizures.

Despite these limitations, our results reveal clear dorso-ventral, time and condition (control/epilepsy) dependent changes in energy metabolism.

Metabolic activity in the dorsal and ventral hippocampus of control mice at ZT3.
At the beginning of the network activation, both dorsal and ventral parts rely on oxidative metabolism, before switching to aerobic glycolysis as metabolic demand increases with activity. Both oxidative metabolism and aerobic glycolysis are larger in the ventral than in the dorsal part. Adding to the dissociation, the dorsal part relies longer on oxidative metabolism. The enhanced metabolic activity in the ventral part may appear surprising since the electrophysiological responses were similar in both dorsal and ventral parts. The local field potential mostly reflects the activation of synapses, whilst the metabolic measurements comprise both postsynaptic and presynaptic events

as well as glial cell activity. A presynaptic mechanism may partly account for the dorso-ventral difference. Although the probability of presynaptic release of both GABA and glutamate is greater in the ventral than in the dorsal hippocampus, the network response to Schaffer collateral activation remains the same[21]. A greater neurotransmitter release probability should increase the metabolic load (e.g. for neurotransmitter recycling). Another contributing factor is the intrinsic excitability, which is greater in the ventral than in the dorsal hippocampus[11, 13, 21]. This is consistent with the greater level of metabolic activity in ventral slices in the absence of stimulation. In addition, glial cells will be highly mobilized, in particular for K^+ and neurotransmitter uptake[59]. The ventral hippocampus contains 1/3 less astrocytes than the dorsal part in rats[60]. Therefore the heavier functional load must be carried by a smaller quantity of astro-glial cells which requires more intense metabolic activity.

Although glucose was immediately used as a substrate for oxidative metabolism in ventral slices, glucose consumption was delayed by 9 s as compared to oxygen in dorsal slices. Alternative substrates include lactate, amino acids, and glycogen. Lactate can be ruled out because we would have measured a decrease in lactate concentration at the beginning of the stimulation, whilst the reversed was observed (Fig. 3C and E). Amino acids, especially glutamate can be metabolized by astrocytes as energy substrates[61]. This scenario is unlikely as, at the beginning of the stimulation, their extracellular concentration should be low. Glycogen is a probable candidate: it is accumulated mainly in astrocytes[62], but it can also be found in smaller quantity in neurons[63] astrocytes in dorsal hippocampus[60] may account for a preferential utilization of glycogen in dorsal region. The glycogen stores are limited[64], therefore glucose needs to be utilized to replenish them, in line with continuous rise in glucose consumption after the end of the synaptic stimulation while oxygen consumption is already declining especially in dorsal hippocampus. The reliance on glycogen in the dorsal hippocampus may be linked to the functions performed in this region. Memory processes that are more specific to the dorsal hippocampus require astrocytic glycogen[65, 66]. Our results do not exclude glycogenolysys in the ventral hippocampus, as it may occur in parallel with glucose uptake. Together, our results show a clear heterogeneity in energy metabolism between the ventral and dorsal parts of the hippocampus at ZT3. This heterogeneity may be linked to the fact that these two regions are implicated in different brain networks and functions[6-8] .

Circadian regulation of metabolic activity in control mice.

Our results show enhanced oxidative glycolysis at ZT8 as compared to ZT3 in particular in ventral slices. Previous works indicate that both NAD(P)H dip and FAD^+ peak reflect the same metabolic processes[48, 67]. Yet, we found an increase in FAD^+ and a decrease in NAD^+ at ZT8 (Fig. 9A, B). This discrepancy can be resolved by the changes in glucose consumption and lactate release, which were larger and smaller at ZT8 than at ZT3 respectively. Importantly, we often observed a decrease in lactate concentration at the beginning of the synaptic stimulation suggesting its uptake. Astrocytic lactate transport is not operational at the measured concentration of 0.1-0.3mM suggesting a lactate uptake by neurons[68]. In neurons, lactate is converted to pyruvate by the lactate dehydrogenase (LDH) that reduces NAD^+ accounting for the observed decrease in NAD(P)H dip amplitude. Since the activity of the glycerol-3-phosphate shuttle is low in neurons[69] or because LDH-derived NADH is spatially distant from the mitochondria, this change in NADH does not affect the mitochondrial $FAD^+/FADH_2$ pool. In parallel, the rapidly available pyruvate will boost the Kreb's cycle increasing NADH. This would explain why NAD^+ and FAD^+ go in opposite directions and argue for increased oxidative metabolism at ZT8.

A metabolic shift toward the preferential use of oxidative metabolism has been observed in many species during sleep[70], and extracellular lactate concentration is a good biomarker of sleep[71]. Circadian changes of energy metabolism may directly reflect the widespread oscillations of the transcriptomic and proteomic landscape[72].

Metabolic activity in slices of dorsal and ventral hippocampus of epileptic mice.

Our results show that the spatial and temporal dimensions are important to consider in order to understand how hippocampal cells produce energy in control animals. Investigating this issue in a pathological context is equally important as metabolic alterations may disrupt cell function, which could lead to cell death and participate to functional deficits, such as memory and learning. Epilepsy is a prototypical example of pathological condition in which metabolic alterations have been identified (see for review[28]). Interestingly, in the animal model we have used, the differences between the ventral and dorsal hippocampus were abolished at ZT3, when seizure probability is low. Since we did not perform a systematic circadian analysis in control animals, we cannot rule out the possibility that such a phenomenon occurs at another ZT in control conditions. Said differently, what we observed at ZT3 in epilepsy would correspond to a phase shift of what happens at another ZT in controls.

We also noted a transient increase in glucose at ZT3 after the stimulation onset. This increase cannot correspond to glucose release, because unlike endothelial cells, glial cells and neurons rapidly phosphorylate glucose to glucose-6-phosphate, thus trapping the substrate in the cell[64]. The most likely possibility is a decrease in glucose uptake. The first step in glycolysis is glucose phosphorylation which requires cytosolic ATP. At the onset of the synaptic stimulation this ATP is also consumed by the Na^+/K^+ ATP-ase pump. Since cells are low in ATP in experimental epilepsy[73], the hexokinase and Na^+/K^+ ATP-ase should compete for ATP. The hexokinase has a lower affinity for ATP (K_m=0.1-0.7mM[74]) than the Na^+/K^+ ATP-ase (K_d=0.1-0.2 μM[75]), which could direct ATP to the pump rather than to the hexokinase, resulting in a decreased glucose uptake. Increases in glucose were more often observed in dorsal (7 from 9) than in ventral slices (3 from 9), which is consistent with the increased excitability of dorsal CA1 pyramidal cells in the pilocarpine model[76] .

Together, the small amplitude of NAD(P)H/FAD^+ signals, glucose, and lactate transients as well as the initial positive deflection of glucose signal suggested a deficient energy metabolism in the both dorsal and ventral parts of the hippocampus in experimental epilepsy, in keeping with the hypometabolism of glucose found in the pilocarpine model of TLE (Kann et al., 2005; Zhang et al., 2015; McDonald et al., 2017). Importantly, the deficit was more pronounced in the ventral than in the dorsal hippocampus. This result is consistent with the fact that neuronal loss, synaptic remodeling, and seizure initiation are more pronounced in the ventral hippocampus[77, 78]

At ZT8, when seizure probability is high, all metabolic signals revealed enhanced aerobic glycolysis as compared to ZT3, the increase being more prominent in the ventral part. In addition, the differences between the dorsal and ventral parts reappeared at ZT8 as compared to ZT3. The time of the day appears as a key parameter to take into account when looking at metabolism in epilepsy, in particular for diagnosis purposes in patients[79]. Enhanced aerobic glycolysis at ZT8 may signal intrinsic enhanced network activity driven by the circadian clock. We can speculate that network activity and metabolism wax and wane in a circadian manner, which may periodically bring networks close to seizure threshold (here in the afternoon).

In conclusion, our results demonstrate that both time and space are key parameters to consider for energy metabolism. Many brain regions develop in a dorsoventral manner[80], leading to heterogeneity in neuron and astrocyte spatial distribution and properties. The dorsoventral differences in energy metabolism may reflect such a diversity as cells are integrated in distinct networks to perform different

tasks. For example, the dorsal and ventral hippocampus are involved in very different functions[6-8]. The time-dependent regulation of metabolism is the second important variable. Body functions are regulated by circadian clocks, which constantly change the molecular organization of cells and circuits. The circadian regulation of metabolism may just be part of this general organization, adapting metabolic needs to cell demands. In epilepsy, the basic principles of a spatiotemporal pattern are still present, but they are considerably modified as compared to the control situation. Whether such modifications are causally related to a phenotype remain to be determined. It is possible that metabolic disturbances may also occur in most, if not all, neurological disorders.

ACKNOWLEDGEMENTS

Supported by A*MIDEX : 2IONXXID/REID/ID17HRU208 and ANR-17-GRF2-0001-03.

FIGURE LEGENDS

Figure 1. A The stimulation of Schaffer collaterals (10Hz during 30s) induced similar LFP responses in slices from dorsal (red traces) and ventral (blue traces) hippocampal regions. **a**: example of an entire LFP response evoked in dorsal and ventral slices. LFP responses were largest at the beginning of stimulation (**b**), decreased with time (**c**) but were still present at the end of the stimulation (**d**).

B. Statistical summary of stimulation parameters and LFP responses to a stimulation train from 10 experiments (10 dorsal and 10 ventral slices, 2 stimulations per slice). **a:** the mean difference between the intensities of current used to produce 50-60% maximum responses in ventral and dorsal slices was 6[-29, 44]µA, demonstrating similar properties regarding the stimulation intensity. **b:** Evolution of the mean integral for each LFP response in the train. The color lines represent the mean values and the light color shading indicates SEM. **c:** Cumulative integrals of LFP responses (trains were given twice in slices) showed similar values in DH and VH. The mean difference between ventral and dorsal slices was 0.11 [-1.07, 1.22]mV*s.

On **Ba** and **Bc** The mean difference between parameter values is shown as a Gardner-Altman estimation plot (see Statistical analysis section of Materials and Methods chapter). The mean difference distribution is plotted on floating gray axes on the right, as a bootstrap sampling distribution (light gray bell shape area). The mean difference is depicted as a black dot; the 95% confidence interval is indicated by the ends of the vertical error bar. Red and blue dashed lines correspond to mean values for dorsal and ventral slices. The 0 point of the mean difference is aligned to the mean value measured in dorsal slices.

Figure 2. Dorso-ventral differences in energy metabolism revealed with imaging NAD(P)H/FAD$^+$ in control animals at ZT3.

A. Comparison of NAD(P)H fluorescence transients recorded in dorsal (red) and ventral (blue) CA1. **a:** Averaged responses for 10 s (dark gray vertical bars) and 30 s (light gray vertical bars) trains. Both trains induced similar global dynamics, with an initial dip followed by an overshoot, and a return to baseline. Traces are averages from 10 independent experiments, with the light color shading indicating the SEM. (**b**) The amplitude of the initial dip was increased in dorsal (blue dots) as compared to ventral (red dots) CA1. (**c**) Although not reaching statistical significance in the 10 s condition, 30 s long trains produced a larger overshoot in ventral than dorsal CA1. Metabolic activity is thus larger in ventral than in dorsal CA1. Experimental data are plotted on the

left axis (**b, c**). The distribution (gray bell-shape) of the differences of mean values of bootstrap samples obtained by resampling of experimental data sets is plotted against the floating gray axis on the right, with the 0 point being aligned to the mean value measured in dorsal CA1 (red dashed line). The black circle with an error-bar shows the mean difference and its 95% confidence interval. Dashed red and blue lines correspond to the mean values of experimental data.

B. Comparison of NAD(P)H transients evoked by 10 s (dashed line) and 30 s(continuous line) trains. **a:** In dorsal slices (red lines) a longer stimulation delayed the overshoot onset (arrow heads) without affecting its amplitude. In ventral slices (blue lines), the overshoot onset times were identical, but the overshoot amplitude was larger with a 30 s train (dashed double-head arrows); **b,c :** Paired comparison of wave shape parameters of NAD(P)H transients evoked using 10 s and then 30 s long trains in dorsal (red dots) and ventral (blue dots) CA1.

C. Comparison of FAD^+ fluorescence transients recorded in dorsal and ventral CA1. **a:** synaptic stimulation with 10 s or 30 s trains produced similar global dynamics in FAD^+ fluorescence, with a larger undershoot amplitude in ventral (blue lines) than dorsal (red lines) CA1. Both initial peak (**b**) and undershoot amplitudes (**c**) were larger in ventral CA1.

D. Comparison of NAD(P)H transients evoked by 10 s (dashed line) and 30 s (continuous line) trains. In dorsal CA1 (**a**, red lines), a longer stimulation delayed the undershoot onset (arrow heads on **a**, red dots on **c**) without affecting its amplitude (**b**, red dots). In ventral CA1 (**a**, blue lines) the undershoot onset times were identical in both cases (**c**, blue dots) but the amplitudes was larger for 30 s long trains (dashed double-head arrows on **a**, blue dots on **b**).

Dark and light gray vertical bars indicate the time of 10s and 30s trains. Since the data set illustrated here passed Shapiro-Francia normality test the unpaired (A, C) and paired (B, D) t-test were used. The p values are expressed as: *- $p<0.05$, **- $p<0.01$, ***- $p<0.001$.

Figure 3. Increased aerobic glycolysis in the ventral hippocampus at ZT3.

A. Mean extracellular oxygen content (pO_2 on left axis, concentration on right axis) is lower in ventral (open circle) than in dorsal (closed circles) slices at all depths ($p<0.0001$, $F=54.3$, $D_{Fn}=1$, $D_{Fd}=72$ two way ANOVA) suggesting higher oxygen consumption in basal conditions.

B. Estimation plots of the mean difference of O_2, glucose and lactate concentration at a

150-200 µm depth between ventral (open circle) and dorsal (closed circles) slices. Metabolic activity is increased in ventral as compared to dorsal CA1 in resting (unstimulated) condition.

C. averaged wave-shapes of the lactate (green), glucose (red), and oxygen (blue) responses to 30 s long trains (gray vertical bar) in dorsal (solid lines) and ventral (dashed lines) slices.

D. Corresponding estimation of the mean differences in amplitude showing larger changes in lactate and glucose concentration in ventral than in dorsal slices, whilst oxygen changes are were similar. **E:** averaged and normalized (to peak amplitude) time courses of glucose (red), oxygen (blue) consumption and lactate (green) release in ventral (upper panel) and dorsal (middle panel) slices. In ventral slices glucose and oxygen consumption started immediately at the onset of synaptic stimulation while in dorsal slices glucose began to change 10 s later. Lactate changes had a similar time course in both types of slices. *- $p<0.05$, **- $p<0.01$ Mann-Whitney test.

Figure 4. Loss of dorso-ventral differences in epilepsy at ZT3.

A. a. The general time course of NAD(P)H was similar in dorsal (red) and ventral (blue) CA1 in pilo mice for both 10 s (dashed lines) and 30 s (continuous lines) long trains. There was no difference in the amplitude of the oxidative dip (**b**) and overshoot (**c**) of NAD(P)H recorded in dorsal (red circles) and ventral (blue circles) slices.

B. a. In both dorsal (red) and ventral (blue) slices, the 30 s long stimulation delayed the onset of the overshoot (**c**) without affecting its amplitude **(b**)**.**

C. a. The general time course of FAD^+ was similar in dorsal (red) and ventral (blue) CA1 in pilo mice for both 10 s (dashed lines) and 30 s (continuous lines) long trains. There was no difference in the amplitude of the oxidative peak (**b**) and undershoot (**c**) of FAD^+ recorded in dorsal (red circles) and ventral (blue circles) slices.

D. In both dorsal (red) and ventral (blue) slices, the 30 s long stimulation delayed the onset of the undershoot (**c**) and increased its amplitude (**b**)**.**

On **Aa** and **Ca**, the averaged trace from 7 independent experiments is displayed; the light color shading indicating the SEM. Dark and light gray vertical bars show the times of 10 s and 30 s trains. Since the data set illustrated here passed the Shapiro-Francia normality test, the unpaired (A, C) and paired (B, D) t-test were used. The p values are expressed as: *- $p<0.05$, ***- $p<0.001$.

Figure 5. Changes in glucose dynamics in epilepsy at ZT3.

A. Basal concentrations of glucose (red) and oxygen (blue) were similar in both slice types while lactate (green) levels were significantly lower in ventral slices.

B. The peaks of lactate, glucose and O_2 concentration in response to 30 s long trains were similar in dorsal and ventral slices. Note that glucose concentration increased at the beginning of synaptic stimulation(gray arrowhead).

C. Time course of averaged transient changes in lactate (green), glucose (red) and oxygen (blue). Traces are normalized to the peak, and polarity changed to make them positive going. In both dorsal and ventral slices, glucose consumption started more than 10 s (double heads dark gray arrow) after the onset of synaptic stimulation (light gray bar).

Since the data sets illustrated here did not pass the Shapiro-Francia normality test, we used the non-parametric Mann-Whitney test. The p values are expressed as: **- $p<0.01$.

Figure 6. Dorsal-ventral differences in NAD(P)H and FAD^+ responses in epileptic mice at ZT8.

A. (**a**) The general time course of NAD(P)H responses were similar in ventral and dorsal CA1. The oxidative peak of NAD(P)H fluorescence was larger in dorsal than ventral CA1 (**b**), while the overshoot was larger in dorsal CA1 (**c**).

B. Increasing the stimulation time increased overshoot amplitude (**a**, double head arrows, **b**) without affecting its onset (**c**) in both regions.

C. (**a**) FAD^+ signals were almost identical in dorsal and ventral CA1. The initial peak amplitude was increased in dorsal CA1 (**b**), while the amplitudes of the undershoot were comparable in both dorsal and ventral CA1 independently from the train duration (**c**).

D. Increasing the stimulation time increased the amplitude of the FAD^+ undershoot (**a**, double head arrows, **b**) with only minor effect on its onset time (**c**).

Aa and **Ca** are averaged from 6 independent experiments; with the light color shading indicating the SEM. Dark and light gray vertical bars show the times of 10 s and 30 s trains. Since the data passed Shapiro-Francia normality test, we used the unpaired (A, C) and paired (B, D) t-test. The p values are expressed as: *- $p<0.05$, **- $p<0.01$, ***- $p<0.001$.

Figure 7. Increased anaerobic glycolysis in ventral CA1 in epileptic mice at ZT8.

A. In basal conditions, tissue concentrations of glucose (red circles) and oxygen (blue circles) were lower in ventral slices suggesting that they consumed more glucose and oxygen that dorsal CA1. There was no detectable regional difference in lactate content.

B. In ventral slices, synaptic stimulation (gray vertical bars) was associated with a larger glucose consumption (red dashed lines and open circles) and lactate release (green dashed lines and open circles) than in dorsal slices (solid lines and closed circles), while oxygen changes were similar(blue lines and circles).

C. Time course of averaged transient changes in lactate (green), glucose (red) and oxygen (blue). Traces are normalized to the peak, and polarity changed to make them positive going. In both ventral and dorsal regions, glucose consumption started later (dark gray arrows) than oxygen, which onset was synchronous to the beginning of the electrical stimulation (vertical gray bar).

Since the data did not pass the Shapiro-Francia normality test, we used the non-parametric Mann-Whitney test. The p values are expressed as: *- $p<0.05$. ***- $p<0.001$.

Figure 8. Accelerated and increased aerobic glycolysis at ZT8 in epileptic mice.

A. a. Comparison of averaged NAD(P)H responses at ZT3 (light color traces) and ZT8 (dark color traces). Two way ANOVA revealed that all parameters describing the wave-shape of NAD(P)H transients (**a**-initial dip amplitude, **c**-overshoot amplitude, **d**-overshoot onset time) depend upon the time of the day (p values indicated in the top left corners of each **b**,**c**,**d** panel), for both ventral and dorsal slices (asterisks show the results of Bonferroni corrected post-hoc t-tests).

B. FAD^+ signals were also time of the day-dependent, but the effect was different between dorsal (warm color traces) and ventral (cold color traces) slices. In particular, the oxidative peak was different in ventral slices only (**a**-gray arrows). Two way ANOVA confirmed that the amplitude of undershoot (**c**) as well as its onset time (**d**) changed as a function of the time of the day (p values in the top left corners of **c**,**d** panels). Post-hoc tests indicated that this variability was significant mainly in ventral slices (asterisks).

C. Oxygen (**a**), glucose (**b**), and lactate (**c**) changes induced by synaptic stimulation in dorsal slices prepared at ZT3 (open circles) and ZT8 (closed circles). Although oxygen consumption did not change at ZT3 and ZT8, glucose concentration was larger (**b**, top panel) and started earlier (**b**, bottom panel) in slices made at ZT8. (**c**) The release of

lactate in ventral slices was increased at ZT8 as compared to ZT3. Since the data in A and B were normally distributer (Shapiro-Francia normality test), we used the unpaired Bonferroni corrected post-hoc t-test. Since experimental data on **C** were not normally distributed, we used the Mann-Whitney test.
The p values are expressed as: *- $p<0.05$, **- $p<0.01$, ***- $p<0.001$.

Figure 9. Dorso-ventral and temporal dissociations in metabolism in control mice.

A. a: Averaged traces of NAD(P)H transients in dorsal and ventral CA1 at ZT3 (light color traces) and ZT8 (dark color traces). (**b**) For dip amplitude a two way ANOVA showed an interaction between two factors, slice type and experimenting time, that means different time regulation for dorsal and ventral slices. The amplitude of overshoot (**c**) as well as its onset time (**d**) varied significantly with time in both slice types (p values in the top left corners of **c**,**d** panels). The Bonferroni corrected post-hoc t-test revealed that all three parameters describing NAD(P)H transients recorded in ventral slices varied with time while only the overshoot onset was modified in dorsal (**b**,**c**,**d** asterisks).

B. a: Averaged traces of FAD^+ transients show higher oxidative peak, as well as a larger and earlier undershoot at ZT8 (dark color traces) than at ZT3 (light color traces). Two way ANOVA confirmed that all these three parameters varied with experimenting time (p values in the top left corners of **b**, **c**, **d** panels) but, this variability was significant in ventral slices only (asterisks).

C. The comparison of glucose, oxygen, and lactate concentration in quiescent and stimulated slices made at ZT8 (closed circles) and at ZT3 (open circles). In slices of both types the resting state glucose (**a**) and oxygen (**c**) concentrations were larger at ZT8 suggesting a lower level of metabolic activity that was consistent with the lower lactate concentration (**e**). Under stimulation conditions, glucose consumption did not vary (**b**) in dorsal slices. However, oxygen consumption (**d**) and lactate release (**g**) were lower at ZT8. In ventral slices, glucose consumption (**b**) was increased while lactate release (**g**) was decreased probably due to lactate consumption as revealed with the concentration dip observed at the beginning of synaptic stimulation (**f**, gray arrow head). Since experimental data on **C** were not normally distributed, we used the Mann-Whitney test.
The p values are expressed as: *- $p<0.05$, **- $p<0.01$, ***- $p<0.001$.

Figure 10. Cartoon illustrating regional (dorsal/ventral) and temporal (ZT3/ZT8) differences in energy metabolism in normal (Control) and epileptic (Pilo) conditions.

A. In control mice the activity of ventral hippocampal cells (neurons/astrocytes) is fueled by aerobic glycolysis which consumes high levels of glucose and produces high levels of NADH. Cytosolic NADH activates the lactate dehydrognase (LDH)-driven conversion of pyruvate to lactate and the mitochondrial glycerol-3-phosphate shuttle (mGPD). Both pathways regenerate cytosolic NAD+ required for the glycolysis. In parallel, mGPD reduces mitochondrial FAD+ that increases the amount of FADH2 available for ATP production by oxidative phosphorylation. In dorsal hippocampal cells, glucose consumption is delayed and long lasting suggesting the utilization and replenishment of glycogen stores. The production of lactate is lower indicating that a large fraction of pyruvate is going to mitochondria via the pyruvate dehydrogenase complex (PDH). The overall metabolic activity in dorsal cell is lower than in ventral.

B. At ZT8, the metabolic activity is increased, in particular in ventral cells. Not only glucose but also lactate are consumed at the onset of synaptic stimulation. The rise in cytosolic NADH resulting from lactate to pyruvate is oxidized by the malate-aspartate shuttle (not shown) that increases the mitochondrial NADH but not $FADH_2$.

C. Energy metabolism activity is decreased in epilepsy, especially in ventral cells. The regional difference disappears at ZT3. Due to the low cytosolic ATP content, the hexokinase activity that reduces glucose utilization is low. Therefore, in both regions the glycolysis is fueled by glycogen which is abundant but has an abnormal structure that prevents its rapid break down. Due to the low glycolysis rate, there is no coupling between cytosolic NADH and mitochondrial $FADH_2$. The energy is produced mainly in mitochondria.

D. At ZT8 the regional difference reappears. In both ventral and dorsal parts aerobic glycolysis is enhanced but in the ventral part glucose consumption and lactate release are larger than in the dorsal part.

References

1. Moujahid, A., D'Anjou, A. & Graña, M. Energy demands of diverse spiking cells from the neocortex, hippocampus, and thalamus. *Front. Comput. Neurosci.* **8**, 41 (2014).

2. Dienel, G. A. Brain Glucose Metabolism: Integration of Energetics with Function. *Physiol. Rev.* **99**, 949-1045 (2019).

3. Levy, W. B. & Baxter, R. A. Energy efficient neural codes *Neural Comput.* **8**, 531-543 (1996).

4. Balasubramanian, V., Kimber, D. & Berry, M. J. Metabolically efficient information processing. *Neural Comput.* **13**, 799-815 (2001).

5. Ames, A. CNS energy metabolism as related to function. *Brain Res. Brain Res. Rev.* **34**, 42-68 (2000).

6. Moser, M. B. & Moser, E. I. Functional differentiation in the hippocampus. *Hippocampus* **8**, 608-619 (1998).

7. Bannerman, D. M. et al. Regional dissociations within the hippocampus--memory and anxiety. *Neurosci. Biobehav. Rev.* **28**, 273-283 (2004).

8. Fanselow, M. S. & Dong, H.-W. Are the dorsal and ventral hippocampus functionally distinct structures? *Neuron* **65**, 7-19 (2010).

9. Dolorfo, C. L. & Amaral, D. G. Entorhinal cortex of the rat: topographic organization of the cells of origin of the perforant path projection to the dentate gyrus. *J. Comp. Neurol.* **398**, 25-48 (1998).

10. Pitkänen, A., Pikkarainen, M., Nurminen, N. & Ylinen, A. Reciprocal connections between the amygdala and the hippocampal formation, perirhinal cortex, and postrhinal cortex in rat. A review. *Ann. N.Y. Acad. Sci.* **911**, 369-391 (2000).

11. Dougherty, K. A., Islam, T. & Johnston, D. Intrinsic excitability of CA1 pyramidal neurones from the rat dorsal and ventral hippocampus. *J. Physiol. (Lond.)* **590**, 5707-5722 (2012).

12. Hönigsperger, C., Marosi, M., Murphy, R. & Storm, J. F. Dorsoventral differences in Kv7/M-current and its impact on resonance, temporal summation and excitability in rat hippocampal pyramidal cells. *J. Physiol. (Lond.)* **593**, 1551-1580 (2015).

13. Malik, R., Dougherty, K. A., Parikh, K., Byrne, C. & Johnston, D. Mapping the electrophysiological and morphological properties of CA1 pyramidal neurons along the longitudinal hippocampal axis. *Hippocampus* **26**, 341-361 (2016).

14. Sotiriou, E., Papatheodoropoulos, C. & Angelatou, F. Differential expression of gamma-aminobutyric acid--a receptor subunits in rat dorsal and ventral hippocampus. *J. Neurosci. Res.* **82**, 690-700 (2005).

15. Pandis, C. et al. Differential expression of NMDA and AMPA receptor subunits in rat dorsal and ventral hippocampus. *Neuroscience* **140**, 163-175 (2006).

16. Sarantis, K., Sotiriou, E., Papatheodoropoulos, C., Matsokis, N. & Angelatou, F. Differential pharmacological properties of GABAA/benzodiazepine receptor complex in dorsal compared to ventral rat hippocampus. *Neurochem. Int.* **52**, 1019-1029 (2008).

17. Marcelin, B. et al. Differential dorso-ventral distributions of Kv4.2 and HCN proteins confer distinct integrative properties to hippocampal CA1 pyramidal cell distal dendrites. *J. Biol. Chem.* **287**, 17656-17661 (2012).

18. Dougherty, K. A. et al. Differential expression of HCN subunits alters voltage-dependent gating of h-channels in CA1 pyramidal neurons from dorsal and ventral hippocampus. *J. Neurophysiol.* **109**, 1940-1953 (2013).

19. Kouvaros, S. & Papatheodoropoulos, C. Major dorsoventral differences in the modulation of the local CA1 hippocampal network by NMDA, mGlu5, adenosine A2A and cannabinoid CB1 receptors. *Neuroscience* **317**, 47-64 (2016).

20. Marcelin, B. et al. Dorsoventral differences in intrinsic properties in developing CA1 pyramidal cells. *J. Neurosci.* **32**, 3736-3747 (2012).

21. Milior, G. et al. Electrophysiological Properties of CA1 Pyramidal Neurons along the Longitudinal Axis of the Mouse Hippocampus. *Sci. Rep.* **6**, 38242 (2016).

22. Kouvaros, S. & Papatheodoropoulos, C. Prominent differences in sharp waves, ripples and complex spike bursts between the dorsal and the ventral rat hippocampus. *Neuroscience* **352**, 131-143 (2017).

23. Ordemann, G. J., Apgar, C. J. & Brager, D. H. D-type potassium channels normalize action potential firing between dorsal and ventral CA1 neurons of the mouse hippocampus. *J. Neurophysiol.* **121**, 983-995 (2019).

24. Thompson, C. L. et al. Genomic anatomy of the hippocampus. *Neuron* **60**, 1010-1021 (2008).

25. Dong, H.-W., Swanson, L. W., Chen, L., Fanselow, M. S. & Toga, A. W. Genomic-anatomic evidence for distinct functional domains in hippocampal field CA1. *Proc. Natl. Acad. Sci. U.S.A.* **106**, 11794-11799 (2009).

26. Jimenez, J. C. et al. Anxiety Cells in a Hippocampal-Hypothalamic Circuit. *Neuron* **97**, 670-683.e6 (2018).

27. Chawla, M. K., Sutherland, V. L., Olson, K., McNaughton, B. L. & Barnes, C. A. Behavior-driven arc expression is reduced in all ventral hippocampal subfields compared to CA1, CA3, and dentate gyrus in rat dorsal hippocampus. *Hippocampus* **28**, 178-185 (2018).

28. Patel, M. A Metabolic Paradigm for Epilepsy. *Epilepsy currents* **18**, 318-322 (2018).

29. Chassoux, F. et al. Determinants of brain metabolism changes in mesial temporal lobe epilepsy. *Epilepsia* **57**, 907-919 (2016).

30. Dubé, C., Boyet, S., Marescaux, C. & Nehlig, A. Relationship between neuronal loss and interictal glucose metabolism during the chronic phase of the lithium-pilocarpine model of epilepsy in the immature and adult rat. *Exp. Neurol.* **167**, 227-241 (2001).

31. Toyoda, I., Bower, M. R., Leyva, F. & Buckmaster, P. S. Early activation of ventral hippocampus and subiculum during spontaneous seizures in a rat model of temporal lobe epilepsy. *J. Neurosci.* **33**, 11100-11115 (2013).

32. Silver, R. & Kriegsfeld, L. J. Circadian rhythms have broad implications for understanding brain and behavior. *Eur. J. Neurosci.* **39**, 1866-1880 (2014).

33. Bailey, S. M., Udoh, U. S. & Young, M. E. Circadian regulation of metabolism. *J. Endocrinol.* **222**, R75-R96 (2014).

34. Eckel-Mahan, K. L. et al. Reprogramming of the circadian clock by nutritional challenge *Cell* **155**, 1464-78 (2013).

35. Greco, C. M. & Sassone-Corsi, P. Circadian blueprint of metabolic pathways in the brain. *Nat. Rev. Neurosci.* **20**, 71-82 (2019).

36. Snider, K. H. & Obrietan, K. Modulation of learning and memory by the genetic disruption of circadian oscillator populations. *Physiology & behavior* **194**, 387-393 (2018).

37. Munn, R. G. K. & Bilkey, D. K. The firing rate of hippocampal CA1 place cells is modulated with a circadian period. *Hippocampus* **22**, 1325-1337 (2012).

38. Nakatsuka, H. & Natsume, K. Circadian rhythm modulates long-term potentiation induced at CA1 in rat hippocampal slices. *Neurosci. Res.* **80**, 1-9 (2014).

39. Snider, K. H. et al. Modulation of learning and memory by the targeted deletion of the circadian clock gene Bmal1 in forebrain circuits. *Behav. Brain Res.* **308**, 222-235 (2016).

40. Snider, K. H., Sullivan, K. A. & Obrietan, K. Circadian Regulation of Hippocampal-Dependent Memory: Circuits, Synapses, and Molecular Mechanisms. *Neural Plast.* **2018**, 7292540 (2018).

41. Manouze, H. et al. Effects of Single Cage Housing on Stress, Cognitive, and Seizure Parameters in the Rat and Mouse Pilocarpine Models of Epilepsy. *eNeuro* **6**, (2019).

42. Ivanov, A., Mukhtarov, M., Bregestovski, P. & Zilberter, Y. Lactate Effectively Covers Energy Demands during Neuronal Network Activity in Neonatal Hippocampal Slices. *Front. Neuroenerg.* **3**, 2 (2011).

43. Harper, A. & Anderson, M. R. Electrochemical glucose sensors--developments using electrostatic assembly and carbon nanotubes for biosensor construction. *Sensors (Basel, Switzerland)* **10**, 8248-8274 (2010).

44. Katsyuba, E., Romani, M., Hofer, D. & Auwerx, J. NAD^+ homeostasis in health and disease *Nature Metabolism* **2**, 9-31 (2020).

45. Efron, B. The bootstrap and modern statistics *J. Am. Stat. Assoc.* **95**, 1293-1296 (2000).

46. Ho, J., Tumkaya, T., Aryal, S., Choi, H. & Claridge-Chang, A. Moving beyond P values: data analysis with estimation graphics. *Nat. Methods* **16**, 565-566 (2019).

47. Lipton, P. Effects of membrane depolarization on nicotinamide nucleotide fluorescence in brain slices. *The Biochemical journal* **136**, 999-1009 (1973).

48. Ivanov, A. I. et al. Glycolysis and oxidative phosphorylation in neurons and astrocytes during network activity in hippocampal slices. *Journal of cerebral blood flow and metabolism : official journal of the International Society of Cerebral Blood Flow and Metabolism* **34**, 397-407 (2014).

49. Langford, D. J. et al. Coding of facial expressions of pain in the laboratory mouse. *Nat. Methods* **7**, 447-449 (2010).

50. Buzsáki, G. Theta oscillations in the hippocampus. *Neuron* **33**, 325-340 (2002).

51. Mello, L. E. et al. Granule cell dispersion in relation to mossy fiber sprouting, hippocampal cell loss, silent period and seizure frequency in the pilocarpine model of epilepsy. *Epilepsy Res. Suppl.* **9**, 51-9; discussion 59-60 (1992).

52. Lévesque, M. & Avoli, M. Carbachol-Induced theta-like oscillations in the rodent brain limbic system: Underlying mechanisms and significance. *Neurosci. Biobehav. Rev.* **95**, 406-420 (2018).

53. Pietersen, A. N. J., Patel, N., Jefferys, J. G. R. & Vreugdenhil, M. Comparison between spontaneous and kainate-induced gamma oscillations in the mouse hippocampus in vitro. *Eur. J. Neurosci.* **29**, 2145-2156 (2009).

54. Malkov, A. et al. Reactive oxygen species initiate a metabolic collapse in hippocampal slices: potential trigger of cortical spreading depression *J. Cereb. Blood Flow Metab.* **34**, 1540-9 (2014).

55. Brennan, A. M., Connor, J. A. & Shuttleworth, C. W. NAD(P)H fluorescence transients after synaptic activity in brain slices: predominant role of mitochondrial function. *Journal of cerebral blood flow and metabolism : official journal of the International Society of Cerebral Blood Flow and Metabolism* **26**, 1389-1406 (2006).

56. Mayevsky, A. & Rogatsky, G. G. Mitochondrial function in vivo evaluated by NADH fluorescence: from animal models to human studies. *American journal of physiology. Cell physiology* **292**, C615-C640 (2007).

57. Giocomo, L. M., Zilli, E. A., Fransén, E. & Hasselmo, M. E. Temporal frequency of subthreshold oscillations scales with entorhinal grid cell field spacing. *Science (New York, N.Y.)* **315**, 1719-1722 (2007).

58. Igarashi, K. M., Ito, H. T., Moser, E. I. & Moser, M.-B. Functional diversity along the transverse axis of hippocampal area CA1. *FEBS Lett.* **588**, 2470-2476 (2014).

59. Boison, D. & Steinhäuser, C. Epilepsy and astrocyte energy metabolism. *Glia* **66**, 1235-1243 (2018).

60. Conejo, N. M. et al. Evidence for sexual difference in astrocytes of adult rat hippocampus. *Neurosci. Lett.* **339**, 119-122 (2003).

61. Dienel, G. A. & McKenna, M. C. A dogma-breaking concept: glutamate oxidation in astrocytes is the source of lactate during aerobic glycolysis in resting subjects. *J. Neurochem.* **131**, 395-398 (2014).

62. Dienel, G. A. & Cruz, N. F. Contributions of glycogen to astrocytic energetics during brain activation. *Metab. Brain Dis.* **30**, 281-298 (2015).

63. Saez, I. et al. Neurons have an active glycogen metabolism that contributes to tolerance to hypoxia. *Journal of cerebral blood flow and metabolism : official journal of the International Society of Cerebral Blood Flow and Metabolism* **34**, 945-955 (2014).

64. Brown, A. M. & Ransom, B. R. Astrocyte glycogen and brain energy metabolism. *Glia* **55**, 1263-1271 (2007).

65. Newman, L. A., Korol, D. L. & Gold, P. E. Lactate produced by glycogenolysis in astrocytes regulates memory processing. *PLoS One* **6**, e28427 (2011).

66. Drulis-Fajdasz, D. et al. Involvement of cellular metabolism in age-related LTP modifications in rat hippocampal slices. *Oncotarget* **6**, 14065-14081 (2015).

67. Shuttleworth, C. W., Brennan, A. M. & Connor, J. A. NAD(P)H fluorescence imaging of postsynaptic neuronal activation in murine hippocampal slices. *J. Neurosci.* **23**, 3196-3208 (2003).

68. Bergersen, L. H. Is lactate food for neurons? Comparison of monocarboxylate transporter subtypes in brain and muscle. *Neuroscience* **145**, 11-19 (2007).

69. McKenna, M. C., Waagepetersen, H. S., Schousboe, A. & Sonnewald, U. Neuronal and astrocytic shuttle mechanisms for cytosolic-mitochondrial transfer of reducing equivalents: current evidence and pharmacological tools. *Biochem. Pharmacol.* **71**, 399-407 (2006).

70. Aalling, N. N., Nedergaard, M. & DiNuzzo, M. Cerebral Metabolic Changes During Sleep. *Curr. Neurol. Neurosci. Rep.* **18**, 57 (2018).

71. Naylor, E. et al. Lactate as a biomarker for sleep. *Sleep* **35**, 1209-1222 (2012).

72. Noya, S. B. et al. The forebrain synaptic transcriptome is organized by clocks but its proteome is driven by sleep. *Science (New York, N.Y.)* **366**, (2019).

73. Melø, T. M., Nehlig, A. & Sonnewald, U. Metabolism is normal in astrocytes in chronically epileptic rats: a (13)C NMR study of neuronal-glial interactions in a model of temporal lobe epilepsy. *Journal of cerebral blood flow and metabolism : official journal of the International Society of Cerebral Blood Flow and Metabolism* **25**, 1254-1264 (2005).

74. Erecińska, M., Nelson, D., Deas, J. & Silver, I. A. Limitation of glycolysis by hexokinase in rat brain synaptosomes during intense ion pumping. *Brain Res.* **726**, 153-159 (1996).

75. Scheiner-Bobis, G. The sodium pump. Its molecular properties and mechanics of ion transport. *Eur. J. Biochem.* **269**, 2424-2433 (2002).

76. Arnold, E. C., McMurray, C., Gray, R. & Johnston, D. Epilepsy-Induced Reduction in HCN Channel Expression Contributes to an Increased Excitability in Dorsal, But Not Ventral, Hippocampal CA1 Neurons. *eNeuro* **6**, (2019).

77. Cavazos, J. E., Jones, S. M. & Cross, D. J. Sprouting and synaptic reorganization in the subiculum and CA1 region of the hippocampus in acute and chronic models of partial-onset epilepsy. *Neuroscience* **126**, 677-688 (2004).

78. Ekstrand, J. J., Pouliot, W., Scheerlinck, P. & Dudek, F. E. Lithium pilocarpine-induced status epilepticus in postnatal day 20 rats results in greater neuronal injury in ventral versus dorsal hippocampus. *Neuroscience* **192**, 699-707 (2011).

79. von Oertzen, T. J. PET and ictal SPECT can be helpful for localizing epileptic foci. *Curr. Opin. Neurol.* **31**, 184-191 (2018).

80. Urbach, R. & Technau, G. M. Dorsoventral patterning of the brain: a comparative approach. *Adv. Exp. Med. Biol.* **628**, 42-56 (2008).

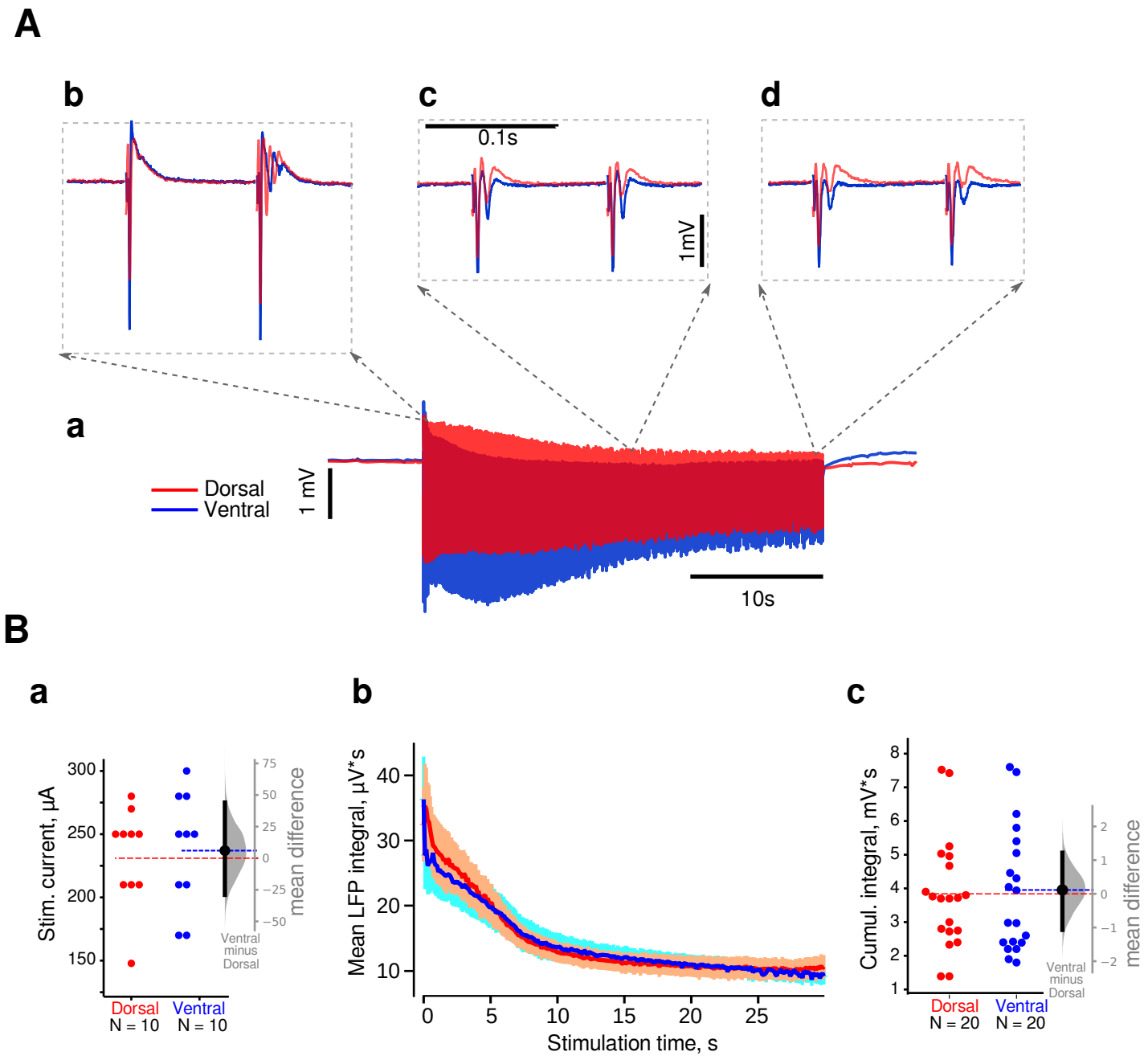
A
b
c
d
0.1s
1mV
a
Dorsal
Ventral
1 mV
10s
B
a
Stim. current, µA
300
250
200
150
75
50
25
0
−25
−50
mean difference
Ventral
minus
Dorsal
Dorsal
N = 10
Ventral
N = 10
b
Mean LFP integral, µV*s
40
30
20
10
0
5
10
15
20
25
Stimulation time, s
c
Cumul. integral, mV*s
8
7
6
5
4
3
2
1
2
1
0
−1
−2
mean difference
Ventral
minus
Dorsal
Dorsal
N = 20
Ventral
N = 20

Figure 1

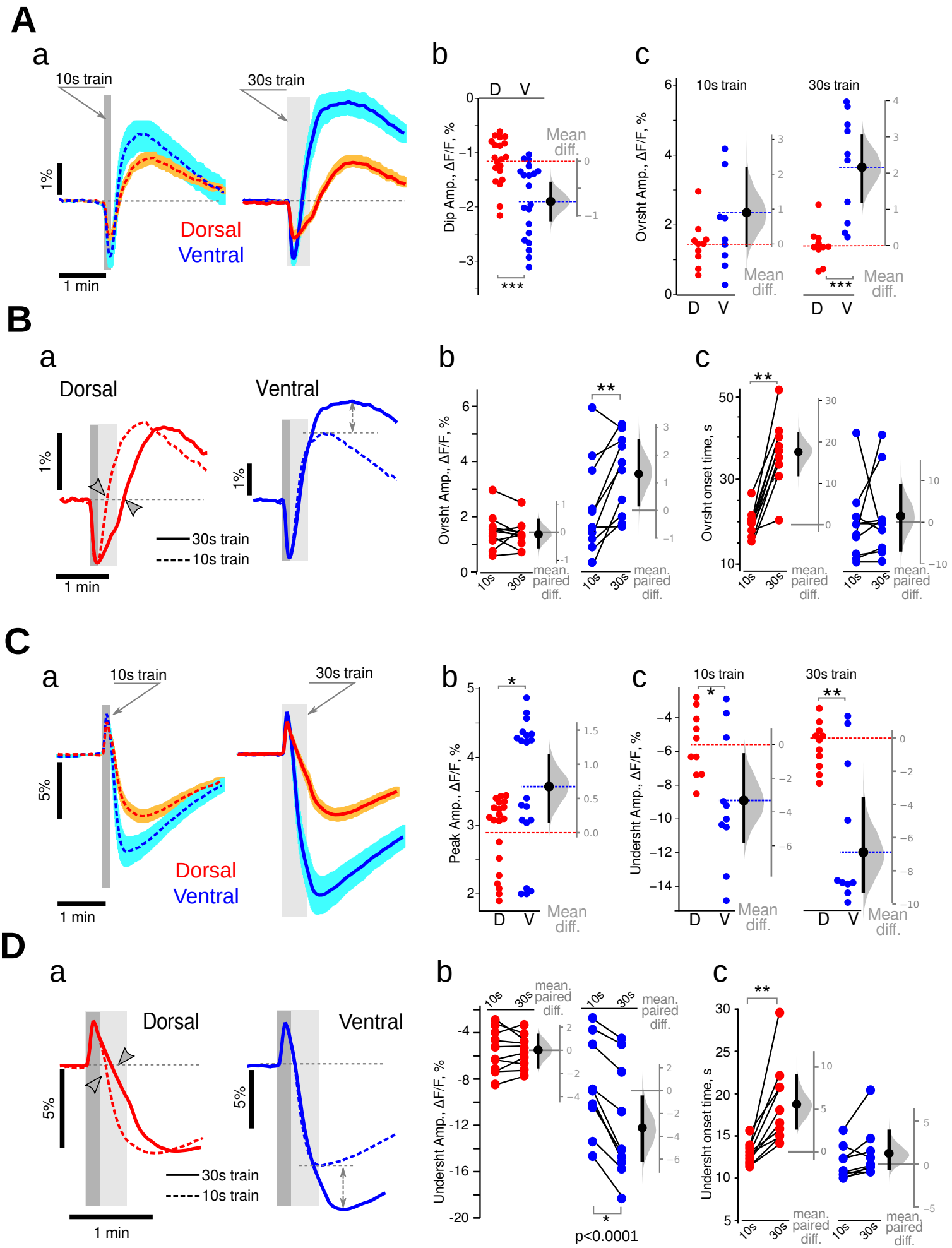
A
a
10s train
30s train
1%
Dorsal
Ventral
1 min
b
D V
Dip Amp., ΔF/F, %
Mean diff.
***
c
10s train
30s train
Ovrsht Amp., ΔF/F, %
Mean diff.
***
B
a
Dorsal
Ventral
1%
30s train
10s train
1 min
b
Ovrsht Amp., ΔF/F, %
**
10s
30s
mean, paired diff.
c
Ovrsht onset time, s
**
C
a
10s train
30s train
5%
Dorsal
Ventral
1 min
b
Peak Amp., ΔF/F, %
*
Mean diff.
c
10s train
30s train
Undersht Amp., ΔF/F, %
*
**
D
a
Dorsal
Ventral
5%
30s train
10s train
1 min
b
Undersht Amp., ΔF/F, %
10s
30s
mean, paired diff.
*
p<0.0001
c
Undersht onset time, s
**

Figure 2

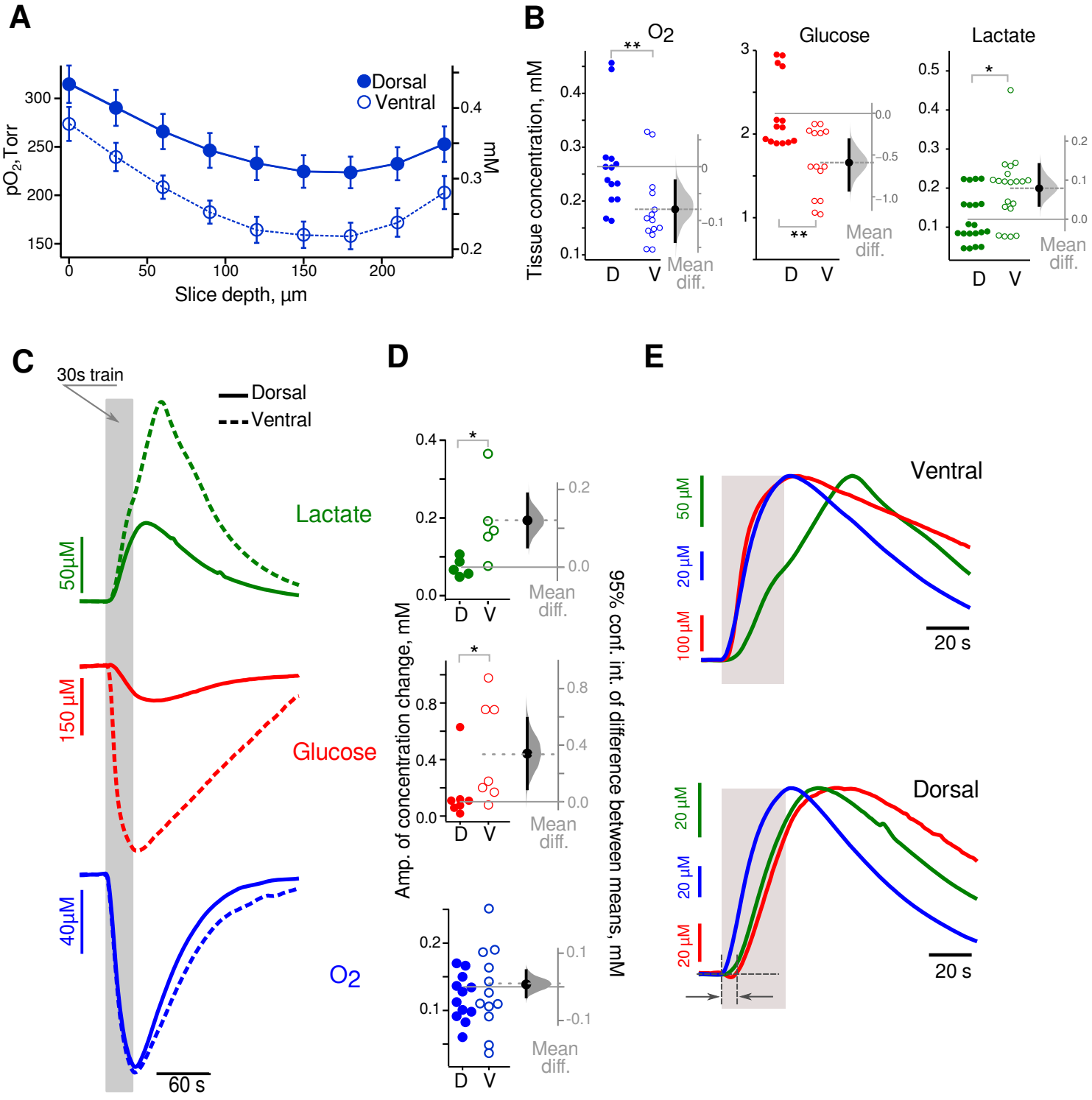
A
Dorsal
Ventral
pO2, Torr
mM
Slice depth, µm
B
O2
Glucose
Lactate
Tissue concentration, mM
Mean diff.
D
V
C
30s train
Dorsal
Ventral
Lactate
Glucose
O2
50µM
150 µM
40µM
60 s
D
Amp. of concentration change, mM
95% conf. int. of difference between means, mM
E
Ventral
Dorsal
50 µM
20 µM
100 µM
20 s

Figure 3

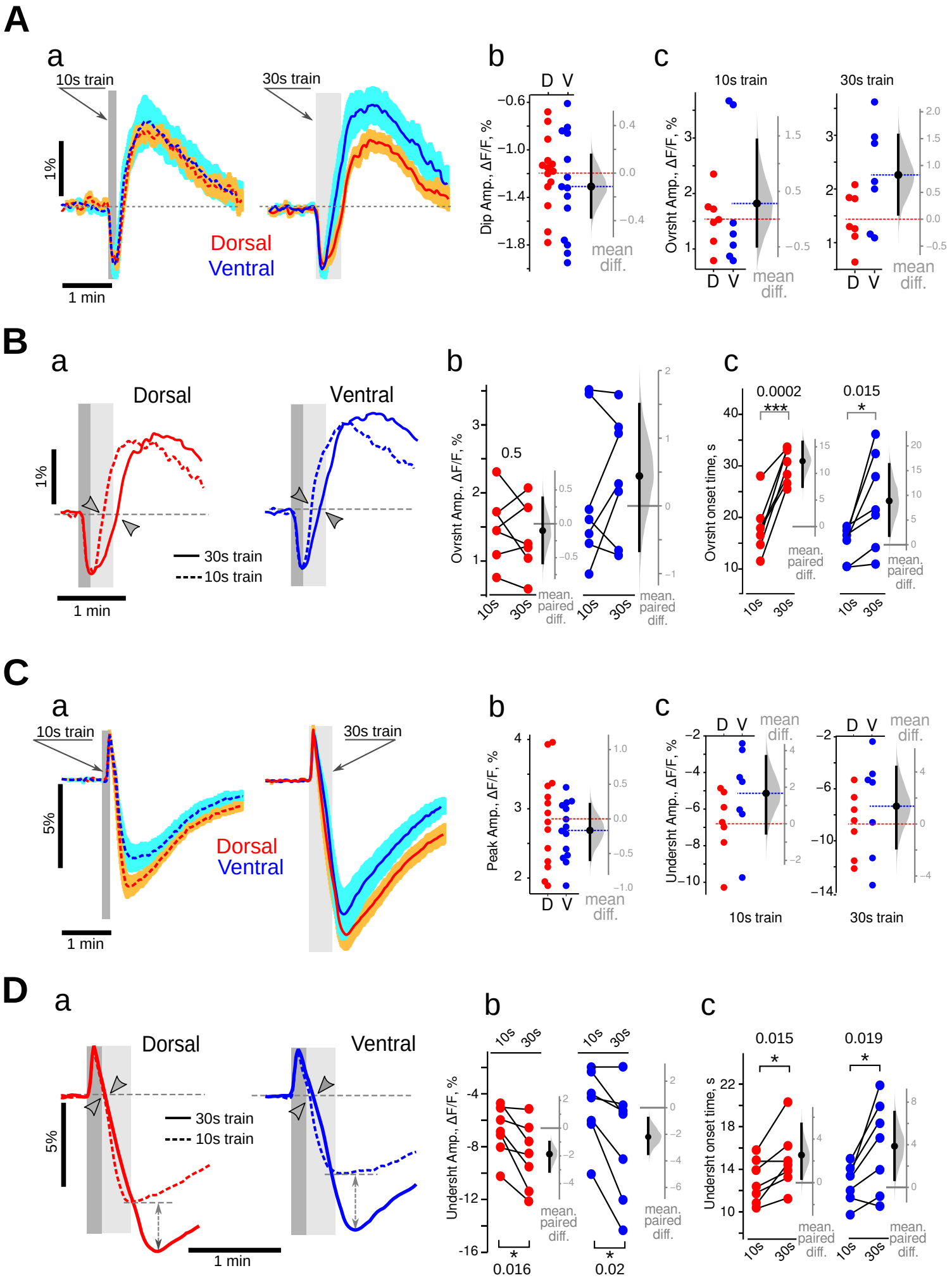
A
a
10s train
30s train
1%
Dorsal
Ventral
1 min
b
D V
Dip Amp., ΔF/F, %
mean diff.
c
10s train
30s train
Ovrsht Amp., ΔF/F, %
D V
mean diff.
B
a
Dorsal
Ventral
1%
30s train
10s train
1 min
b
Ovrsht Amp., ΔF/F, %
0.5
10s
30s
mean. paired diff.
c
0.0002
0.015
***
*
Ovrsht onset time, s
C
a
10s train
30s train
5%
Dorsal
Ventral
1 min
b
Peak Amp., ΔF/F, %
D V
mean diff.
c
Undersht Amp., ΔF/F, %
10s train
30s train
D
a
Dorsal
Ventral
5%
30s train
10s train
1 min
b
Undersht Amp., ΔF/F, %
10s 30s
*
0.016
0.02
c
0.015
0.019
Undersht onset time, s
mean. paired diff.

Figure 4

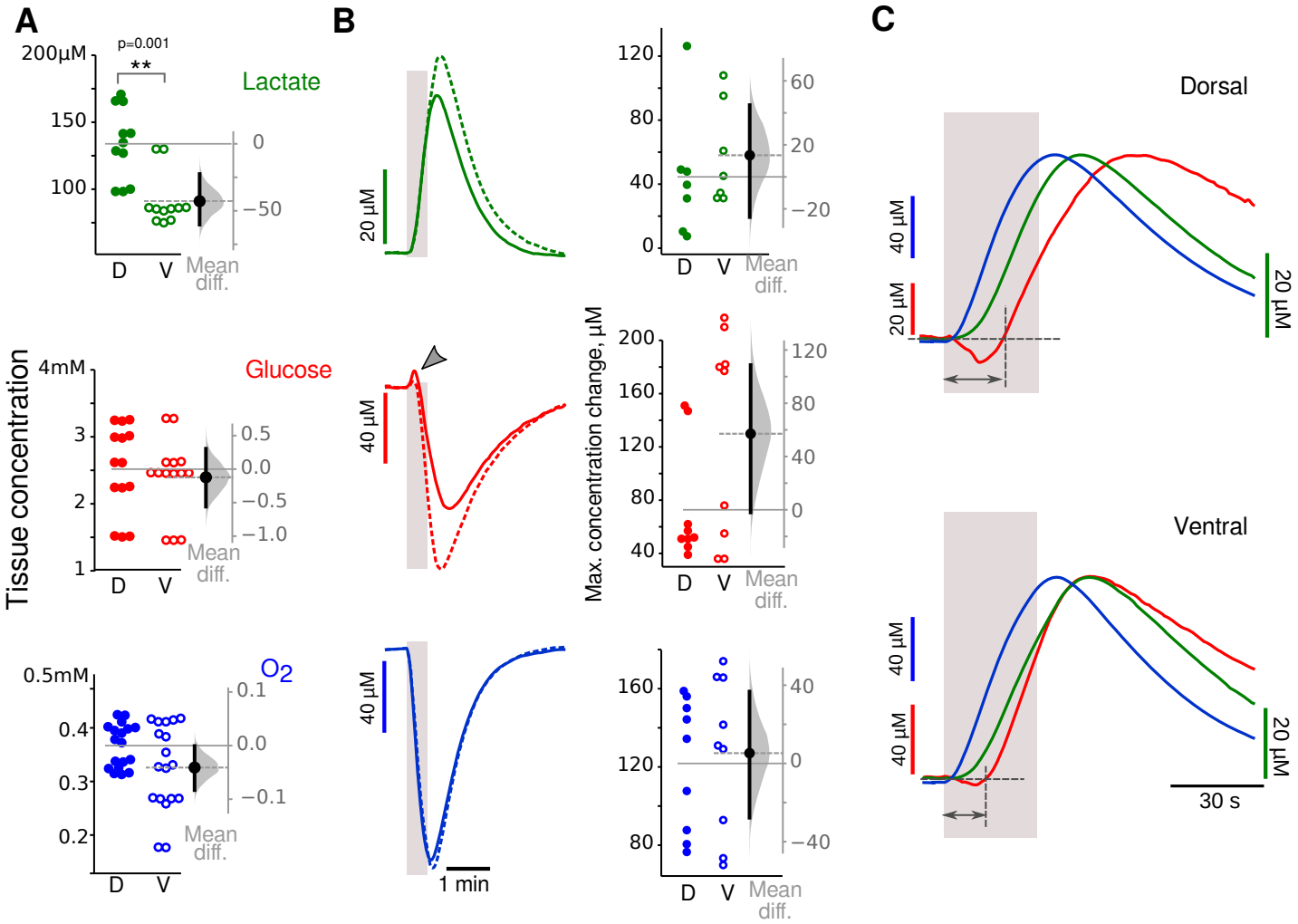
A
B
C
Lactate
Glucose
O2
Tissue concentration
200µM
150
100
4mM
3
2
1
0.5mM
0.4
0.3
0.2
p=0.001
**
D
V
Mean diff.
0
−50
0.5
0.0
−0.5
−1.0
0.1
0.0
−0.1
20 µM
40 µM
1 min
Max. concentration change, µM
120
80
40
0
60
20
−20
200
160
120
80
40
0
40
0
−40
Dorsal
Ventral
30 s

Figure 5

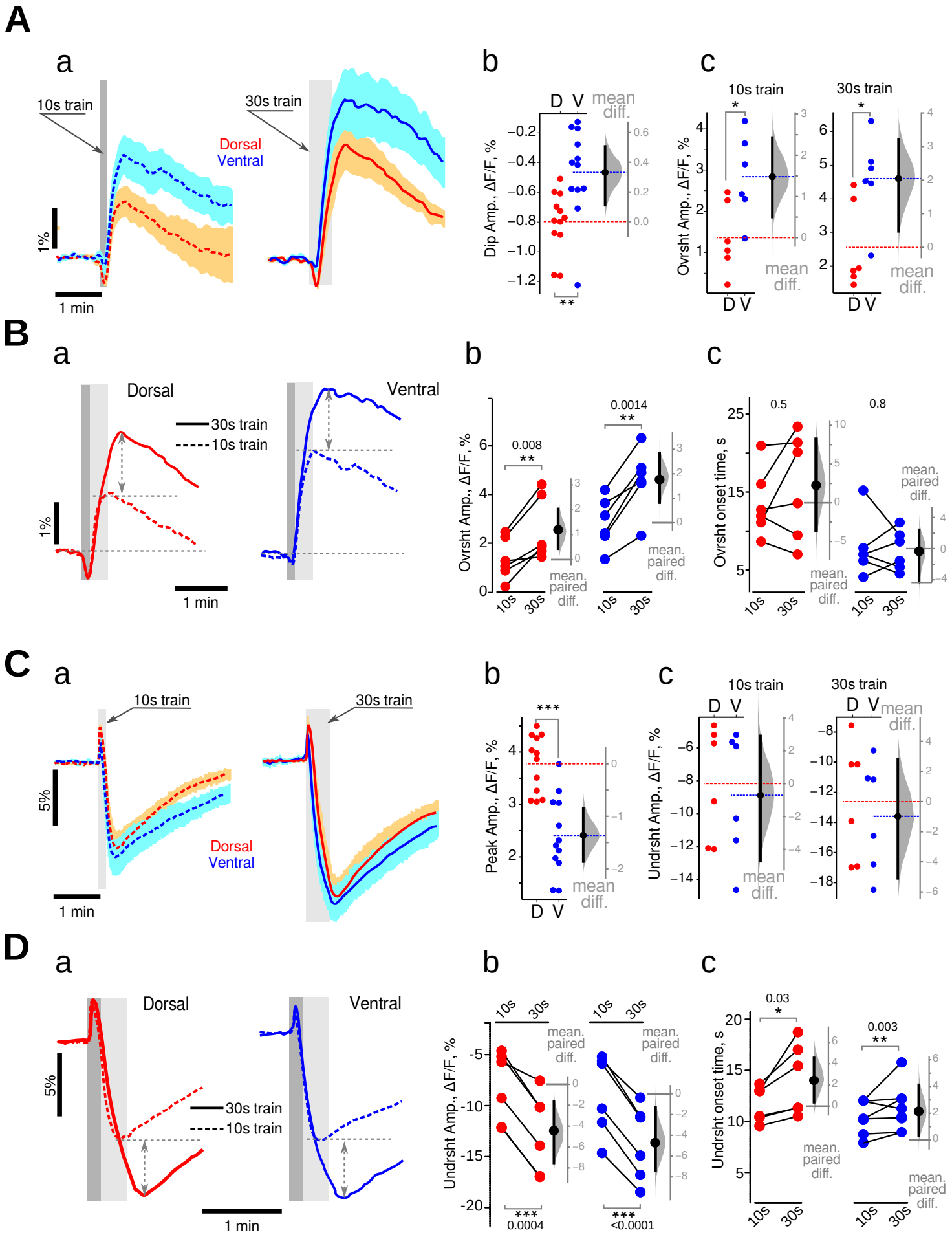
A
a
10s train
30s train
Dorsal
Ventral
1%
1 min
b
D V
mean diff.
Dip Amp., ΔF/F, %
**
c
10s train
30s train
Ovrsht Amp., ΔF/F, %
*
mean diff.
B
a
Dorsal
Ventral
30s train
10s train
1%
1 min
b
Ovrsht Amp., ΔF/F, %
0.008
**
0.0014
**
mean. paired diff.
10s
30s
c
Ovrsht onset time, s
0.5
0.8
C
a
10s train
30s train
5%
Dorsal
Ventral
1 min
b
Peak Amp., ΔF/F, %
***
mean diff.
c
Undrsht Amp., ΔF/F, %
D
a
Dorsal
Ventral
5%
30s train
10s train
1 min
b
Undrsht Amp., ΔF/F, %
***
0.0004
***
<0.0001
c
Undrsht onset time, s
0.03
*
0.003
**

Figure 6

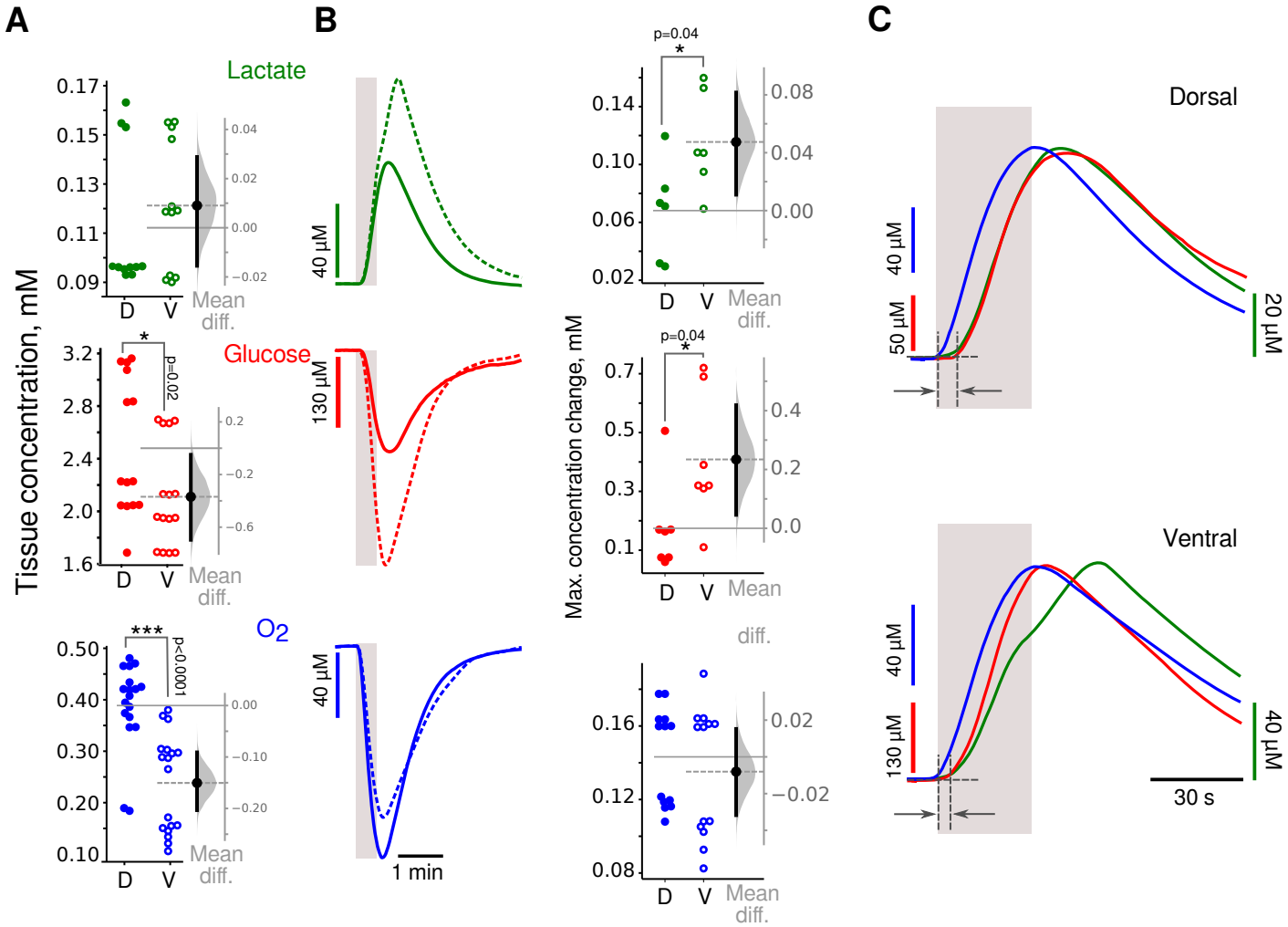
A
B
C
Lactate
Glucose
O2
Tissue concentration, mM
Max. concentration change, mM
D
V
Mean diff.
p=0.02
p<0.0001
p=0.04
40 µM
130 µM
1 min
Dorsal
Ventral
50 µM
20 µM
30 s

Figure 7

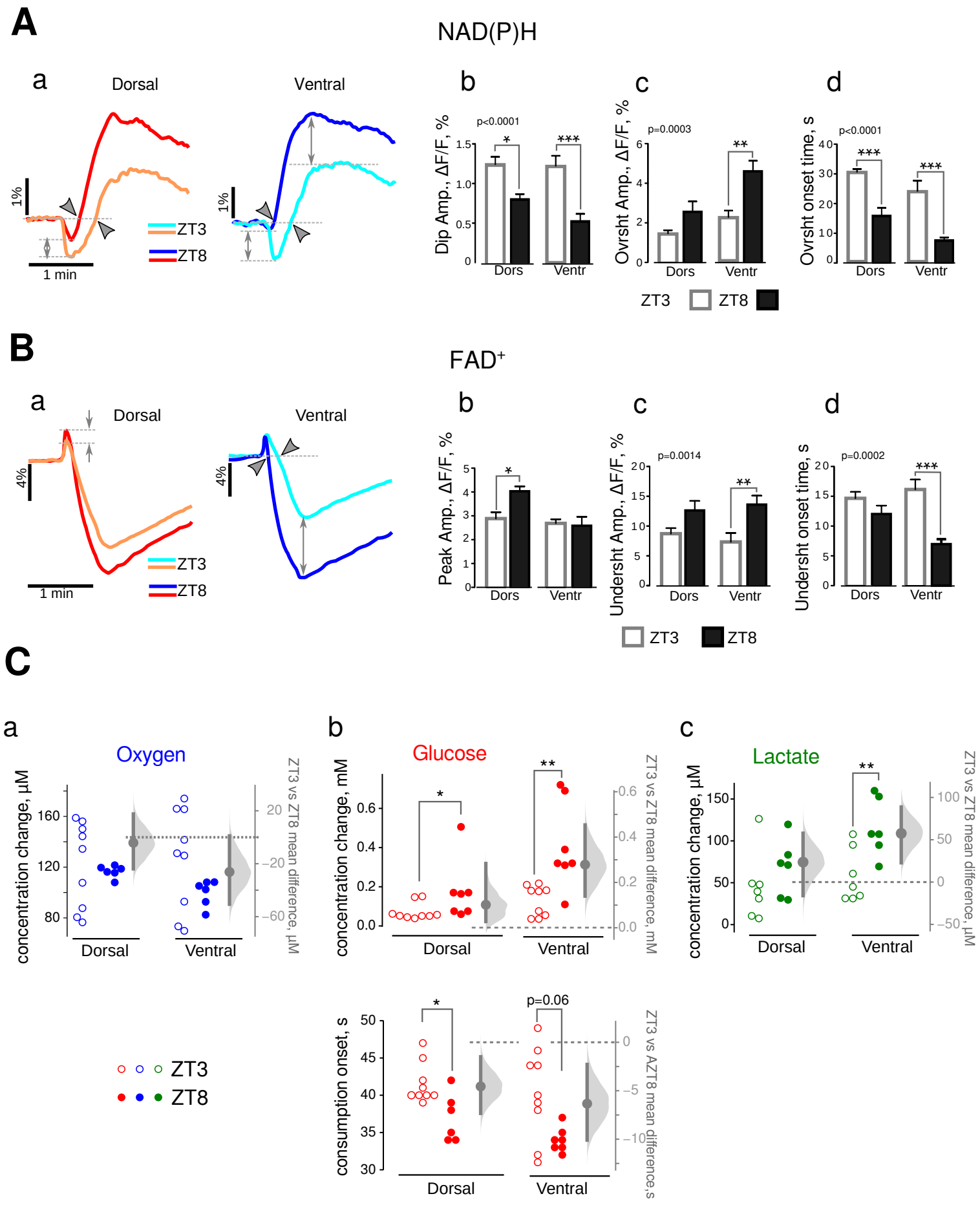
A
NAD(P)H
a
Dorsal
Ventral
1%
1 min
ZT3
ZT8
b
Dip Amp., ΔF/F, %
p<0.0001
*
***
Dors
Ventr
c
Ovrsht Amp., ΔF/F, %
p=0.0003
**
d
Ovrsht onset time, s
p<0.0001
***
B
FAD+
4%
Peak Amp., ΔF/F, %
Undersht Amp., ΔF/F, %
p=0.0014
Undersht onset time, s
p=0.0002
C
Oxygen
concentration change, µM
ZT3 vs ZT8 mean difference, µM
Glucose
concentration change, mM
ZT3 vs ZT8 mean difference, mM
Lactate
consumption onset, s
p=0.06
ZT3 vs AZT8 mean difference,s

Figure 8

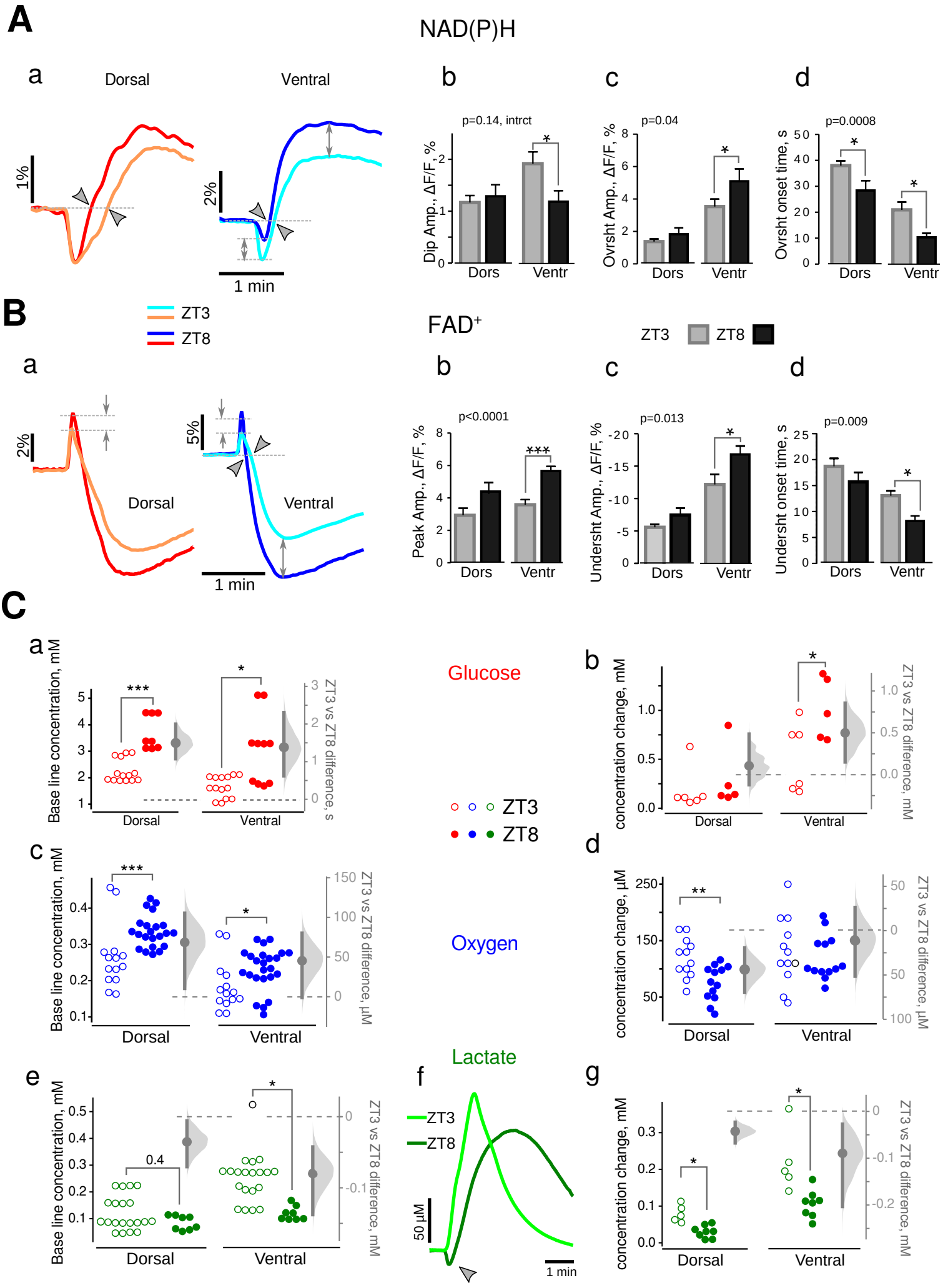
A
NAD(P)H
a
Dorsal
Ventral
1%
2%
1 min
b
p=0.14, intrct
Dip Amp., ΔF/F, %
Dors
Ventr
c
p=0.04
Ovrsht Amp., ΔF/F, %
d
p=0.0008
Ovrsht onset time, s
B
ZT3
ZT8
FAD+
ZT3
ZT8
p<0.0001
Peak Amp., ΔF/F, %
p=0.013
Undersht Amp., ΔF/F, %
p=0.009
Undersht onset time, s
C
Glucose
Base line concentration, mM
concentration change, mM
ZT3 vs ZT8 difference, s
ZT3 vs ZT8 difference, mM
Oxygen
Base line concentration, mM
concentration change, μM
ZT3 vs ZT8 difference, μM
Lactate
ZT3
ZT8
50 μM
1 min
Base line concentration, mM
concentration change, mM
ZT3 vs ZT8 difference, mM

Figure 9

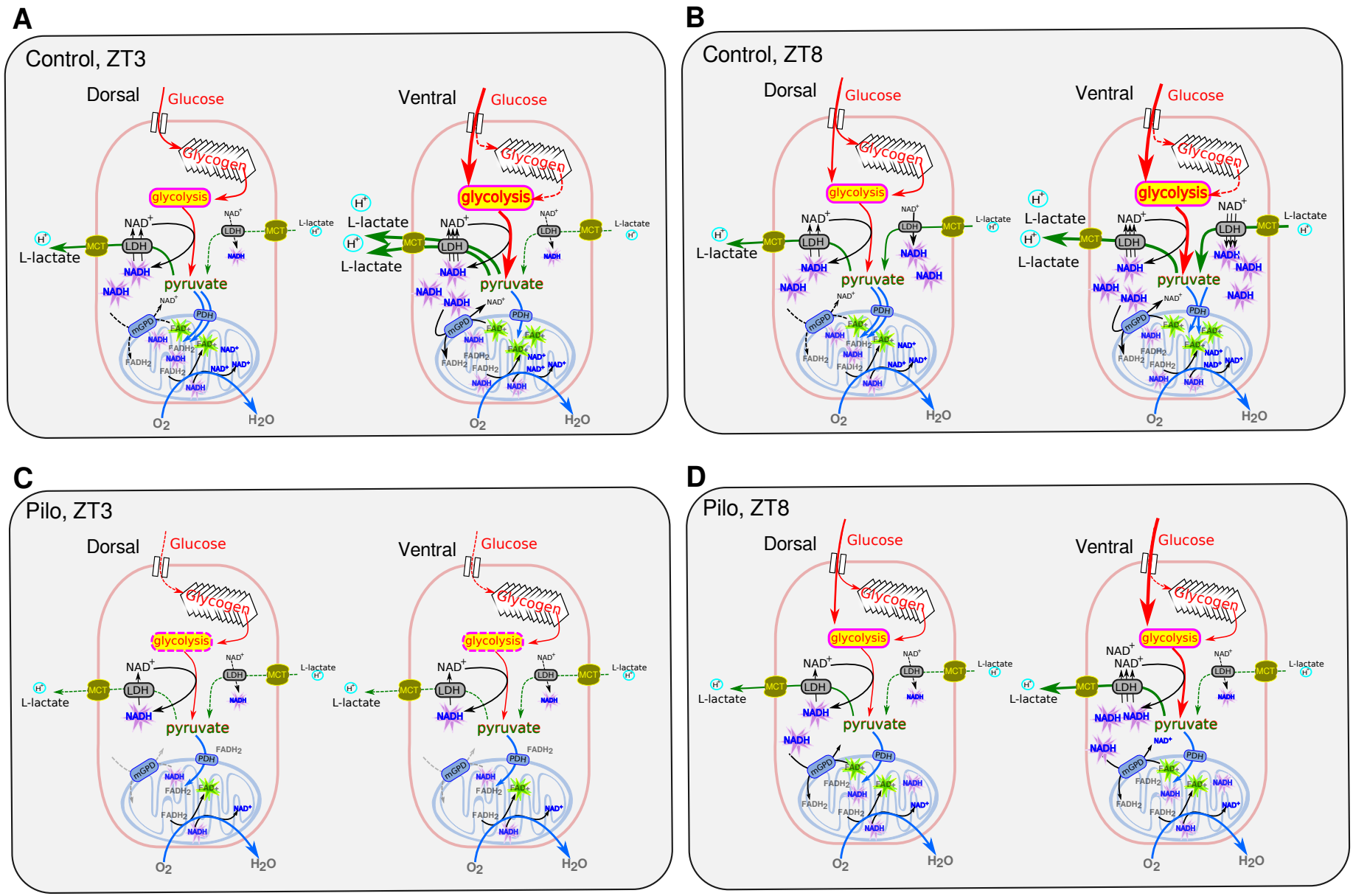
A
Control, ZT3
Dorsal
Ventral
Glucose
Glycogen
glycolysis
pyruvate
L-lactate
MCT
LDH
NAD+
NADH
PDH
mGPD
FAD+
FADH2
O2
H2O
B
Control, ZT8
C
Pilo, ZT3
D
Pilo, ZT8